nature geoscience

SUPPLEMENTARY INFORMATION

DOI: 10.1038/NGEO1548

"Regional climate control of glaciers in New Zealand and Europe during the pre-industrial Holocene"

Aaron E. Putnam, Joerg M. Schaefer, George H. Denton, David J.A. Barrell,

Robert C. Finkel, Bjørn G. Andersen, Roseanne Schwartz,

Trevor J.H. Chinn, Alice M. Doughty

Table of Contents **Page no.**

Table of Contents (cont.) **Page no.**

1.0 Geologic and climatic setting

The Cameron Glacier is a temperate mountain glacier draining a ~6 km^2 mountain catchment on the southeast side of the Arrowsmith Range (Fig. S1). The bedrock of the Arrowsmith Range is indurated quartzofeldspathic sandstone (greywacke) and mudstone (argillite) of the Triassic-age Torlesse Composite Terrane[1]. The Arrowsmith Range is a 10 km-long rugged northeast-southwest-trending mountain chain, lying about 15 km southeast of the main drainage divide ('Main Divide') of the central Southern Alps. The Southern Alps form a 500 km-long barrier to the prevailing westerlies, creating an orographic precipitation regime. Mean annual precipitation rises rapidly from 3 m at the seaward edge of the narrow western coastal plains to a maximum of at least 10 m in the western part of the Southern Alps close to the Main Divide. From there, precipitation diminishes approximately exponentially to about 1 m in the eastern part of the Southern Alps. Precipitation on the Arrowsmith Range is estimated to be about 3 m (water equivalent) per year[2].

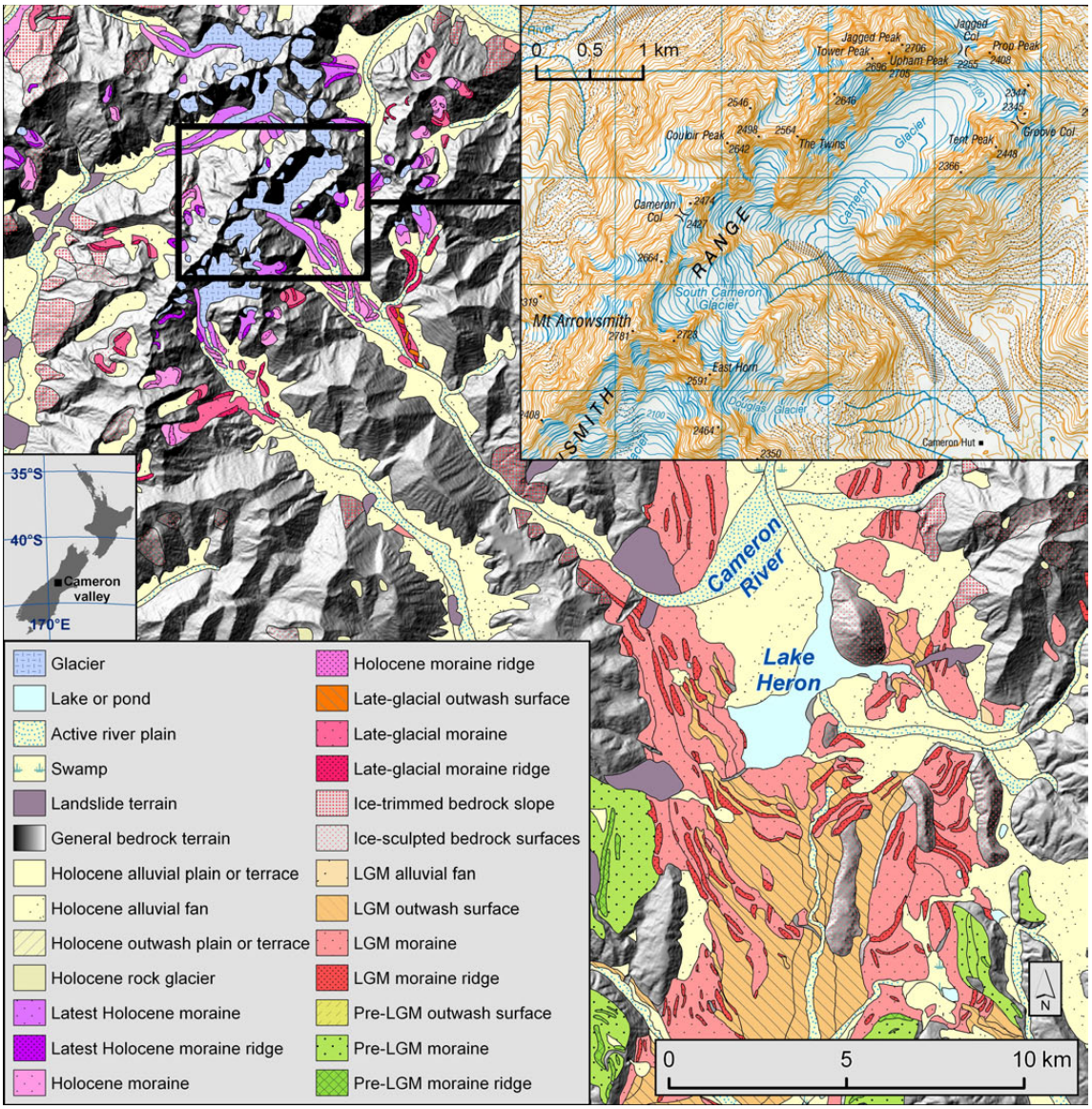

Figure S1. Geomorphologic map of Cameron River valley, northern Arrowsmith Range, Lake Heron valley, and surrounding region (adapted from ref. 3). Topographic map of the northern Arrowsmith Range, including Cameron Glacier, is inset.

2.0 Physiographic description of the Cameron Glacier catchment

The Cameron Glacier catchment (Fig. S1) includes the highest peaks in the Arrowsmith Range: Jagged Peak (2706 m a.s.l.), Couloir Peak (2642 m a.s.l.), and Mount Arrowsmith (2781 m a.s.l.). The bulk of the Cameron Glacier flows from the northeast part of the catchment, and is joined by ice streams flowing from Coulior Peak and Cameron Col. The accumulation area of the Cameron Glacier in AD2006 was about 0.94 km^2, and the total area was 1.91 km^2. These area values should be considered in the context of recent general snowline rise and consequent glacier disequilibrium. High in the southwest sector of the catchment, draining Mt Arrowsmith and East Horn, is the South Cameron Glacier, which does not currently contribute ice to the Cameron Glacier, except perhaps by snow or ice avalanching. Abutting the South Cameron Glacier catchment to the south is Douglas Glacier, one of 47 index glaciers in the Southern Alps for which end-of-summer snowlines have been recorded since the AD1970s[4]. An estimated mean equilibrium-line altitude (ELA; hereafter 'snowline') of 2120 m a.s.l., inferred from the altitude mid-point of the glacier, was assigned to the Douglas Glacier by Chinn[4]. This value was derived from 20 m-interval topographic contours on late 20th century 1:50,000 scale topographic maps (Land Information New Zealand map series NSMS 260 and NZTopo50). Snowline fluctuations on the Douglas Glacier exhibit a strong correlation ($r = 0.91$) to snowline changes averaged across the Southern Alps[5]; thus the Douglas Glacier snowline is well representative of regional snowline changes across the Southern Alps. Because of its proximity to the Cameron Glacier catchment,

we take the snowline of the Douglas Glacier as an approximation of the Cameron Glacier snowline.

A key reference position for analysis of the Cameron Glacier system, present and past, is the mid-19th century terminus of the Cameron Glacier, documented in AD1864 by means of a pen-and-wash drawing by the geologist of the Canterbury Province, Julius von Haast[6] (see Fig. S11). Subsequent observations show the glacier terminus to have receded progressively since that time. By AD1964, the terminus was ~0.8 km inside the AD1864 position, and by AD1989 had retreated a further ~0.4 km (ref. 7). The terminus underwent an additional net recession of ~0.4 km between AD1989 and AD2006. This duration of net ice retreat includes a period in the mid-1990s in which the Cameron Glacier terminus paused or slightly readvanced[3,8].

3.0 Geomorphology of the Cameron Glacier moraine system

3.1 Geomorphic setting

The 16–km-long valley of the Cameron River drains southeast from the Arrowsmith Range, before entering the large intermontane Lake Heron basin (Fig. S1). The Cameron valley floor is as much as 1 km wide, though in places narrows to as little as 200 m where constricted by large alluvial fans emerging from tributary valleys.

The moraine system of the Cameron valley was studied over many years by Colin Burrows, who assigned names and ages to the various components of the moraine system[7,9,10]. The innermost belt of moraines, named the Arrowsmith moraines by

Burrows[9], lie ~0.5 km down valley from the present-day position of the Cameron Glacier terminus. Lying between 0.5 km and about 1.1 km downstream of the AD1864 terminus is the next-oldest belt of moraines, named Inner Marquee, while the Outer Marquee moraines extend for a further 0.75 km down-valley. Farther outboard is the Wildman moraine belt, comprising a complex of latero-terminal moraines and associated outwash surfaces. The Wildman moraine terminus lies about 3.5 km down the valley axis from the AD1864 terminus. In the wider context, the Wildman moraine terminus is about 6 km down-valley of the catchment head, and 10 km upstream of where the Cameron valley debouches into the Lake Heron basin.

During the Last Glaciation, ice from the Cameron valley coalesced with a lobe of ice from the Rakaia valley, in what is now the Lake Heron basin, producing prominent sets of terminal and lateral moraines, and outwash plains[3,11,12]. Prominent lateral moraines in the lower part of the Cameron valley, near where it enters the Lake Heron basin, are as much as 400 m above the present valley floor, and attest to the thickness of ice flowing from the Cameron catchment during the Last Glaciation.

3.2 Age of the Wildman moraines

The Wildman moraines (W) are older than the Marquee moraines, and are characterised by notably better developed soil profiles than occur on the Marquee moraines[7,9]. The Wildman moraines have long been assumed to be of late-glacial age, and correlation has been suggested to the Birch Hill moraines of the Waitaki River catchment[9,13] that have recently been shown to be ~13,000 yrs old[14]. Just downstream of

the Wildman terminal moraine ridges, Burrows[9] documented a stratigraphic exposure of a buried soil developed on a Wildman outwash terrace, overlain by colluvium, and reported a ^{14}C age of 9520 ± 95 ^{14}C yrs (N.Z. 688) on a piece of wood from the buried soil. This ^{14}C age converts to a calendar age of 10,860 ± 164 cal. yrs BP (i.e., 'years before AD1950', hereafter just 'yrs') using the OxCal 4.1 program[15] and the IntCal09 curve[16], and affords a minimum age for the Wildman outwash surface. This sits compatibly with the age reported in this paper for the oldest of the Outer Marquee moraines of about 10,700 yrs, which also offers a minimum age for the Wildman moraines.

3.3 Detailed description of the Marquee and Arrowsmith moraine sequences

Here we describe the geomorphology of these moraines. We then use mapped and described moraine morphology to (a) deduce information about the former behaviour of the Cameron Glacier terminus, and (b) reconstruct former snowlines from which atmospheric palaeo-temperatures can be calculated. The Cameron Glacier moraine system comprises a remarkably well-preserved set of adjacent ridges that mark culminations of former expansions of the Cameron Glacier (Figs. S2, S3, and S4). We targeted this moraine set for Holocene climate reconstruction because of the pristine quality and large number of relatively young (i.e., younger than late-glacial age) terminal moraines suitable for snowline reconstruction. Holocene moraines occur sequentially along the axis of the Cameron valley floor over a distance of 5.3 km from the outermost moraines to the AD2006 position of the Cameron Glacier terminus (Figs. S2, S3, and S4). Cross-cutting relationships exhibited by nearly all of the moraines indicate that almost

every moraine ridge was formed at the culmination of a glacier advance. Such excellent preservation of terminal moraines is uncommon in the Southern Alps, and is probably because of downcutting, rather than meandering, of the Cameron River since the moraine set was formed. Such downcutting spared terminal moraines situated on the valley bottom from destruction or burial under outwash by the Cameron River.

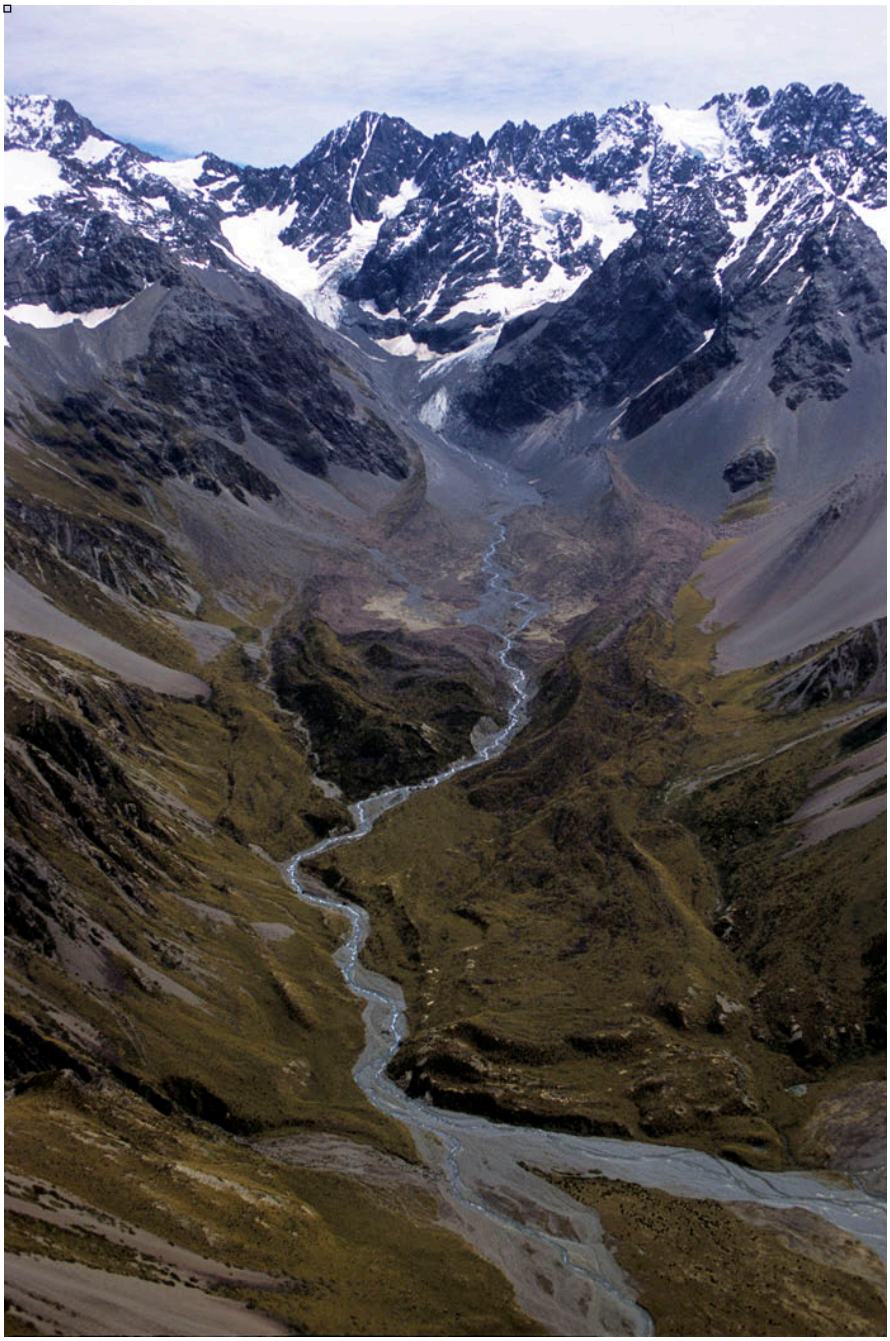

Figure S2. Aerial photograph of the Cameron valley moraines from ridge C3 to modern (AD2006) ice margin. Wildman moraines lie down-valley of this view. Vantage is northwest. The AD2006 terminus of the Cameron Glacier is at the valley head and the Holocene moraines are in the middle and foreground. Imagery date: January, AD2006.

Figure S3. Aerial photograph of the middle sector of the Cameron valley moraines. Pink-stained ridges are the 'Arrowsmith' moraines and vegetated ridges are the 'Inner Marquee' moraines. Vantage is northwest. Imagery date: January, AD2006.

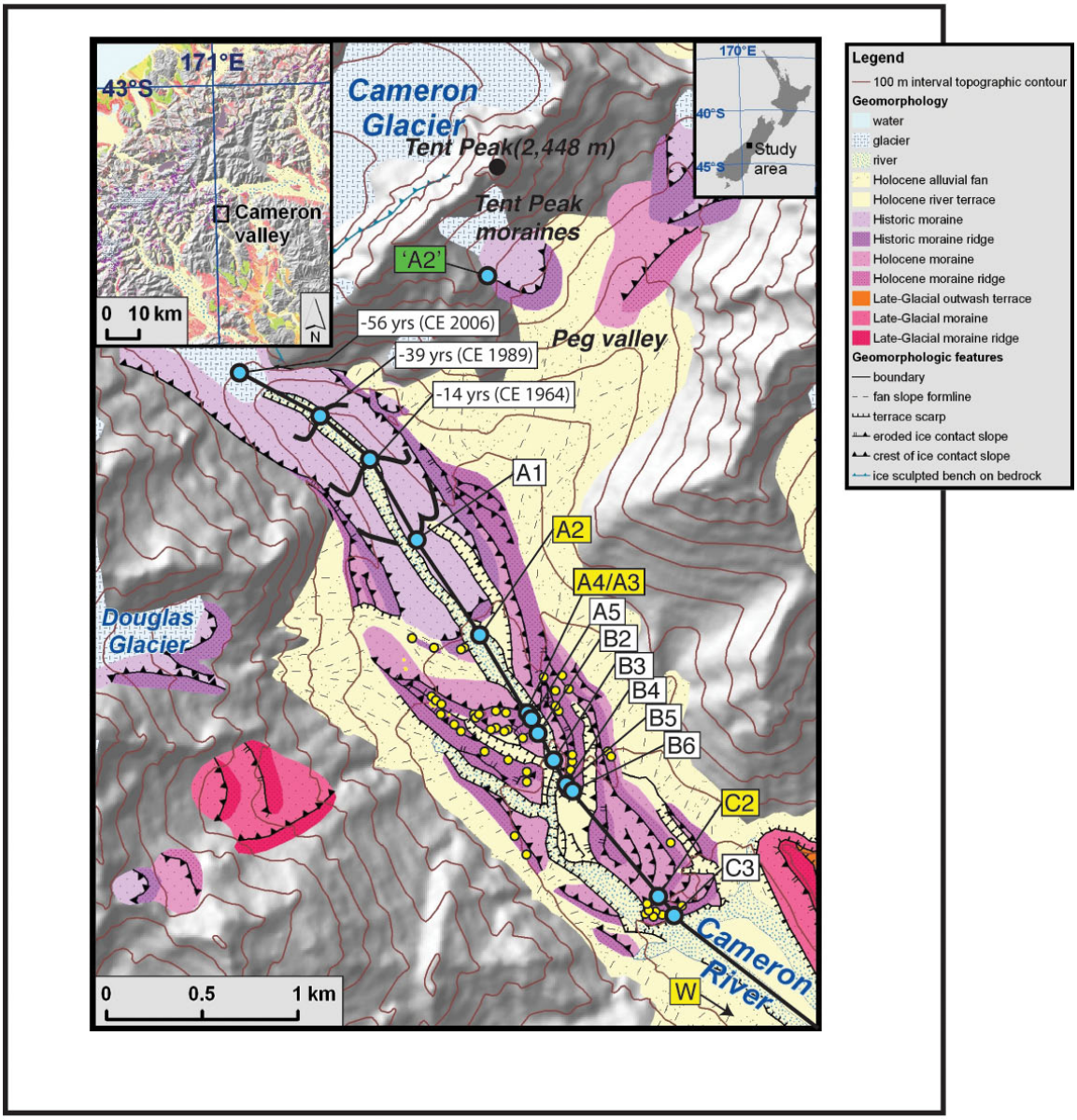

Figure S4. Glacial geomorphic map of the Cameron Glacier moraine system (refer to Fig. 1 in main text for dating results). Dated moraine designations are given in boxes and shown by blue dots. Black line trending along Cameron valley axis forms the basis for moraine distance measurements, discussed in text. Yellow-filled boxes indicate moraines chosen for AAR palaeo-snowline reconstructions. Green-filled box indicates geomorphic correlation between the Tent Peak moraine and the A2 moraine.

3.3.1 The Outer Marquee moraines

This succession of moraines, lying 1.7 km upvalley from the inner Wildman terminal moraine ridge (Figs. S4 and S5), was named the 'Marquee' (M) moraines by Burrows[9]. They exhibit overlapping morpho-stratigraphic relationships, indicating that each ridge was formed during culmination of successive, progressively less-extensive advances of Cameron Glacier. The outermost moraines (mapped as moraines C6-C2 by Burrows[9]) have ridges ~2-10 m high, and moraine surfaces exhibit 30-50 cm-deep podsolic, yellowish-brown soils that support vegetation similar to that found on the Wildman moraines[7]. Marquee moraine ridge C2 overprints ridge C3 where the terminal moraine transitions into left- and right-lateral ridges, suggesting that C2 was deposited at the culmination of glacier advance. Numerous greywacke boulders occur embedded in and resting in stable positions on the C5-C2 moraine ridges. Boulders exhibit reddish surface staining, quartz veins raised as much as 10 mm above surrounding rock surface, ~3.0-mm thick weathering rinds, and large lichens.

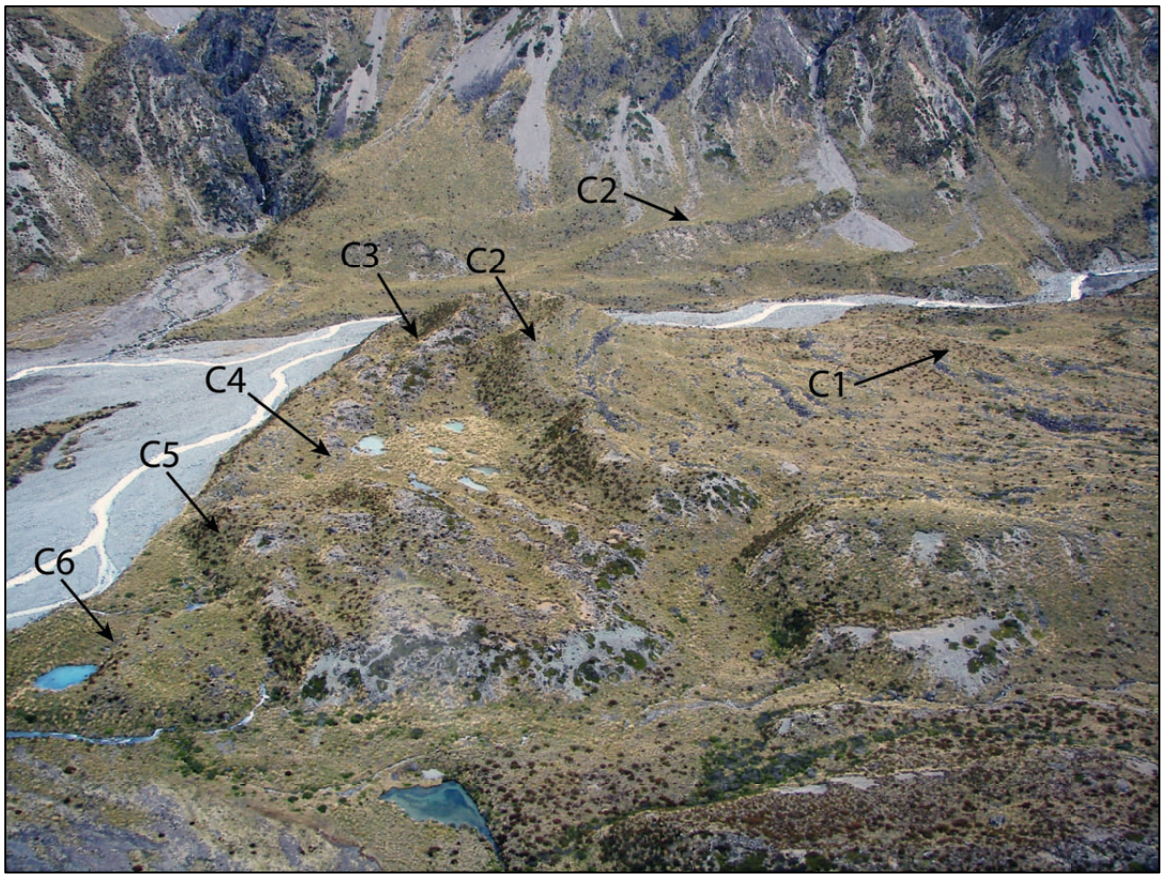

Figure S5. Aerial photograph of moraines C6-C1 (arrowed from left to right, respectively). Vantage is southwest. When producing the moraines, the Cameron Glacier flowed from the right side of the image. Imagery date: April, AD2006.

3.3.2 The Inner Marquee moraines

About 0.65 km inboard of the C2 terminal ridge is the outer limit of the inboard set of vegetated moraines called the 'Inner Marquee' moraines by Burrows[9] (Figs. S4 and S6). This moraine complex consists of seven prominent nested latero-terminal moraines, five of which contained boulders suitable for ^{10}Be dating (Fig. S6). Moraine ridges of this complex support 20-50 cm of podsolic brown soils, and vegetation similar to that found on the Wildman and outer Marquee moraines. Boulders feature weathering rinds 2.5-3.0 mm thick and quartz veins rising as much as 6 mm from the surrounding boulder surface. Boulder surfaces support *Rhizocarpon geographicum* and *R. candidum* lichen as

wide as 30.7 cm and 27.9 cm, respectively[9]. This complex features a 340-m-long left-lateral ridge segment (B5[9]) that overprints part of the C2 left-lateral moraine ridge. This segment is truncated at its southernmost extent by the inboard B4 and B3 lateral ridges, but the B5 moraine appears to re-emerge south of where the B4 lateral moraine transitions into a terminal ridge.

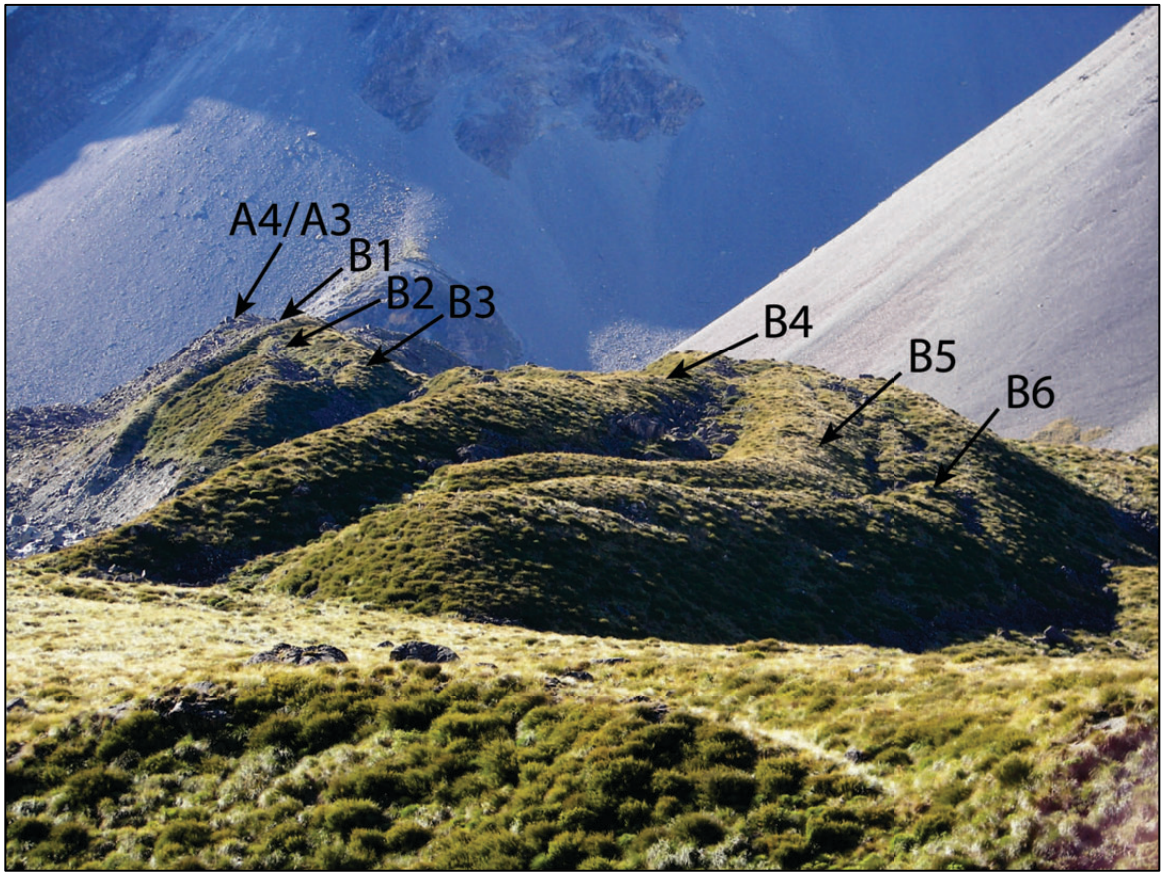

Figure S6. View northeast toward the 'Inner Marquee' moraine complex of Burrows[9]. Terminal moraines B6 to B1, and A4/A3 are visible from right to left (arrowed). Ridge A3, with a notably less vegetated appearance, overprints the complex to the far left (arrowed). Glacier flow was from the image left. Imagery date: March, AD2007.

The B4 moraine is a prominent 2-8 m tall ridge that crosscuts the B5 and B6 terminal loops just east of the Cameron River (Fig. S4). This ridge can be traced west across the Cameron River, where the terminal B4 moraine overprints the B5 segment

described above. The B5 moraine can then be traced continuously for 0.51 km up valley as a right-lateral moraine ridge.

The B3 right-lateral moraine ridge overlaps and obscures the northernmost extent of B4 (Figs. S4 and S7). This ridge tracks 0.59 km southward over the B4 moraine ridge in the northern section, and along the B4 right-lateral ice-contact slope in the southern section, to where B3 loops into a terminal moraine ridge. The B3 moraine is truncated at its southernmost extent by a prominent meltwater channel graded to the A4 moraine ridge.

Figure S7. Photograph of the small bouldery ridge of B3. Ridge (arrowed) is set within ice-contact slope of B4, which occupies the foreground. Vantage is southeast. Ridges B4, C1, C2, and W2 are visible in background. Imagery date: April, AD2006.

Located immediately inboard of B3, the prominent 2-3 m tall B2 right-latero-terminal moraine is the innermost of the vegetated and soil-covered moraines (Figs. S4 and S7). Ridge B2 overprints the northern extent of B3. The B2 ridge can be traced continuously southward to where the moraine loops into a terminal ridge. At its southernmost extent, the A4 meltwater channel truncates B2. The B2 ridge can be traced across the meltwater channel to a small terminal moraine ridge segment that is likely the continuation of the former B2 moraine before dissection by A4 meltwater.

3.3.3 The Arrowsmith moraines

A distinct set of less soil-covered and more sparsely vegetated moraines occurs inboard of the Inner Marquee moraines in the Cameron valley. Burrows[9] named this innermost set the 'Arrowsmith' moraines. The outermost ridge of the Arrowsmith set, the A5 moraine, is a 0.22-km long and 9-14 m tall 'ear-shaped' terminal loop located just inboard of B2 on the west side of the Cameron River (Figs. S4 and S8). Podsolic grayish-brown soils 10-20 cm deep[7] occur sporadically across the bouldery surface of the A5 moraine. Shrubs occurs in patches and consist of *Chionochloa* sp., *Celmisia* sp., *Dracophyllum uniflorum*, and *Podocarpus nivalis*[7]. Salient boulders are only slightly weathered compared to those on the Wildman and Marquee moraines. Boulder surface rind thicknesses are ~0.75 mm. Surface boulders are stained pink and feature quartz veins that are flush with the surrounding matrix. *R. geographicum* and *R. candidum* lichen growing on boulder surfaces have maximum thalli widths of 20.3 cm and 10.7 cm, respectively.

Figure S8. Photograph with vantage west toward where moraine A5 (arrowed vegetated ridge in foreground) is overprinted by A4/A3 (light-colored bouldery ridge in middle ground; arrowed). Ridge A4/A3 also overprints B2 (background; arrowed). Glacier flow was from the right. Imagery date: April, AD2006.

The A5 ridge has been obscured at both its eastern and western ends by the prominent ~14-m tall A4 terminal moraine ridge, implying that A4 marks the culmination a glacier advance (Figs. S3, S4, S8, and S9). The A4 ridge [labeled variably 'A3' and 'A4' by Burrows [9], and hence a possible composite moraine ridge] can be traced for 0.99 km from the northernmost right-lateral extent, to where the moraine grades into a terminal loop. The terminal moraine has been truncated by the Cameron River gorge at its southernmost extent, but the prominent pink bouldery ridge can be traced eastward across the river to where the terminal ridge grades into a left-lateral moraine. The left

lateroterminal ridge can be traced 1.63 km north (up valley) to where it merges with the A2 left-lateral ridge, forming a steep lateral moraine of composite age. The bouldery A4 moraine surface supports 'very immature' 0-15 cm deep grayish-brown soils [7] with scattered patches of *Dracophyllum pronum*, *Gaultheria crassa*, and *Racomitrium lanuginosum*[7] shrubs. Boulders on the A4/A3 moraine feature 0.75 mm weathering rinds. Quartz veins are flush with boulder surfaces. *R. geographicum* and *R. candidum* lichens growing on boulder surfaces have maximum widths of 11.7 and 7.3 cm, respectively.

In the early 1970s, Burrows[9] identified a stratigraphic section along the eastern bank of the Cameron River that exposed a buried wood-bearing soil that he inferred to be related to the timing of formation of the A4 moraine. Burrows et al.[7] later provided a reinterpretation of the stratigraphy of the site, and suggested that the buried soil overlies the ice-contact surface of the thin A3/A4 moraine, and that outwash capping the buried soil grades to an inboard moraine ('A2b'). A ^{14}C measurement on wood from this buried soil yielded an age of 537 ± 50 ^{14}C yrs (N.Z. 687). This date converts to calendar age of 527 ± 36 yrs [1σ; calculated using OxCal 4.1[15] and the SHCal04 calibration curve[17]], and is considered a minimum age for abandonment of the A4 ice-contact slope.

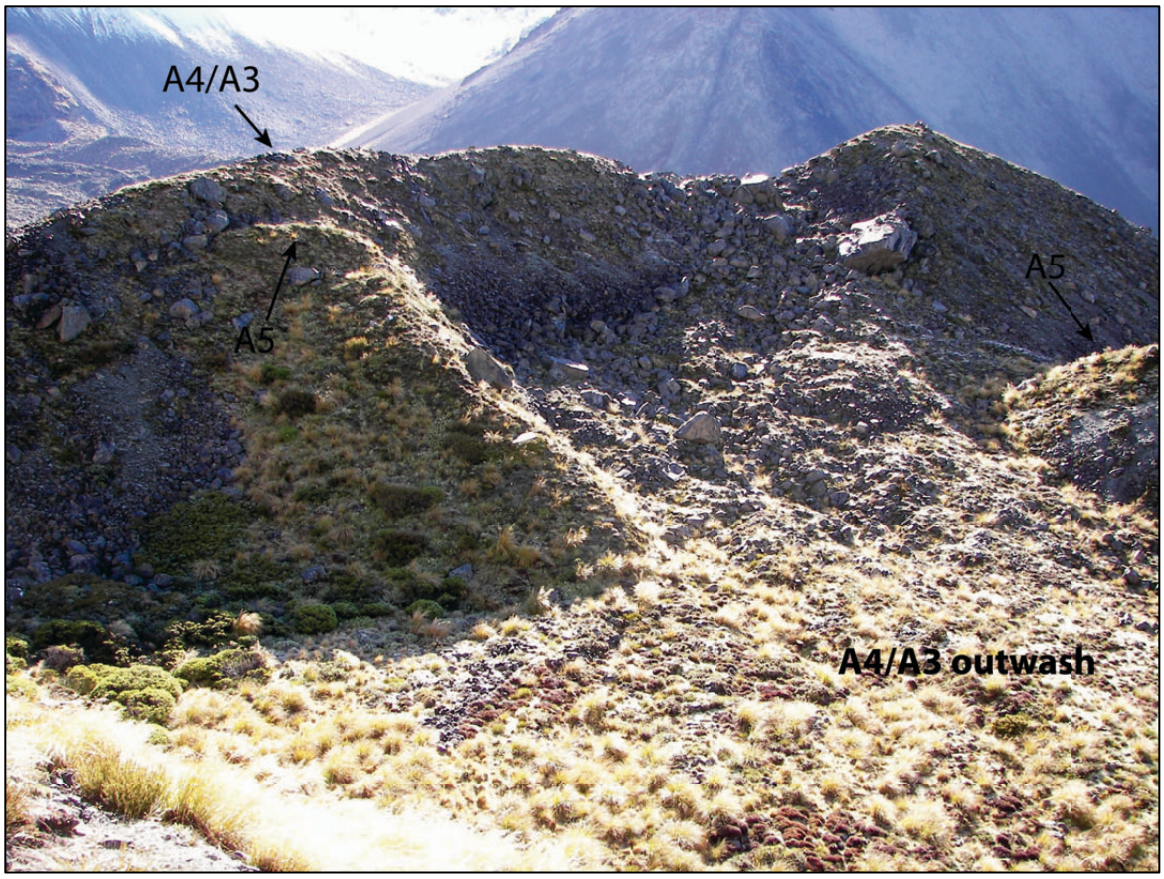

Figure S9. Photograph of the distal side of A4/A3. Vantage is north. When it sat at the A4/A3 moraine position (arrowed), the Cameron Glacier generated a meltwater stream ('A4/A3 outwash') that breached the A5 moraine ridge (arrowed) and produced the impressive channel and the bouldery outwash fan, visible in the center to lower left. Imagery date: April, AD2006.

After construction of the A4 moraine, the Cameron Glacier terminus receded by at least 0.50 km. Subsequent advance of the Cameron Glacier terminus led to construction of the low (1-2 m), discontinuous A2 moraine ridge at a position 0.50 km inboard of the A4 ridge (Figs. S3, S4 and S10). The A2 moraine is a terminal loop that grades into a right-lateral moraine ridge that can be traced ~0.4 km up-valley before the moraine is overwhelmed by alluvium and colluvium at the base of the western valley wall. To the east, the A2 moraine grades into a prominent continuous left-lateral moraine that can be traced 1.0 km to where the moraine merges with the A4/A3 lateral moraine

ridge to become a left-lateral moraine of composite age. The bouldery, clast-supported A2 moraine surface contains sporadic immature grayish brown soils supporting herbaceous vegetation, including *Epilobium* sp., *Poa novae-zelandiae*, *Raoulia* sp., and various mosses[7]. Boulder surfaces are mostly fresh and grey, with slight rust-colored staining. Weathering rinds are ~0.2 mm and quartz veins are flush with the rock surface. *R. geographicum* lichen are ~3.2 cm in diameter, whereas no *R. candidum* has been documented[7]. The left-lateral portion of the A2 moraine overlaps a continuous semi-parallel moraine located 1-2 m outboard ('A2b'). At its southern section, the A2 moraine overprints and obscures the outboard ridge.

Haast's AD1864 pen-and-wash drawing shows that at that time the Cameron Glacier was positioned near the A2 moraine ridge, roughly even with the Peg tributary valley east of the Cameron River[6,9] (this image can be viewed online at: http://find.natlib.govt.nz/). It is unclear from the drawing whether the ice margin documented by Haast[6] produced the A2 moraine or if the glacier was slightly inboard. Sometime after AD1864 the Cameron Glacier terminus retreated a minimum distance of 0.46 km.

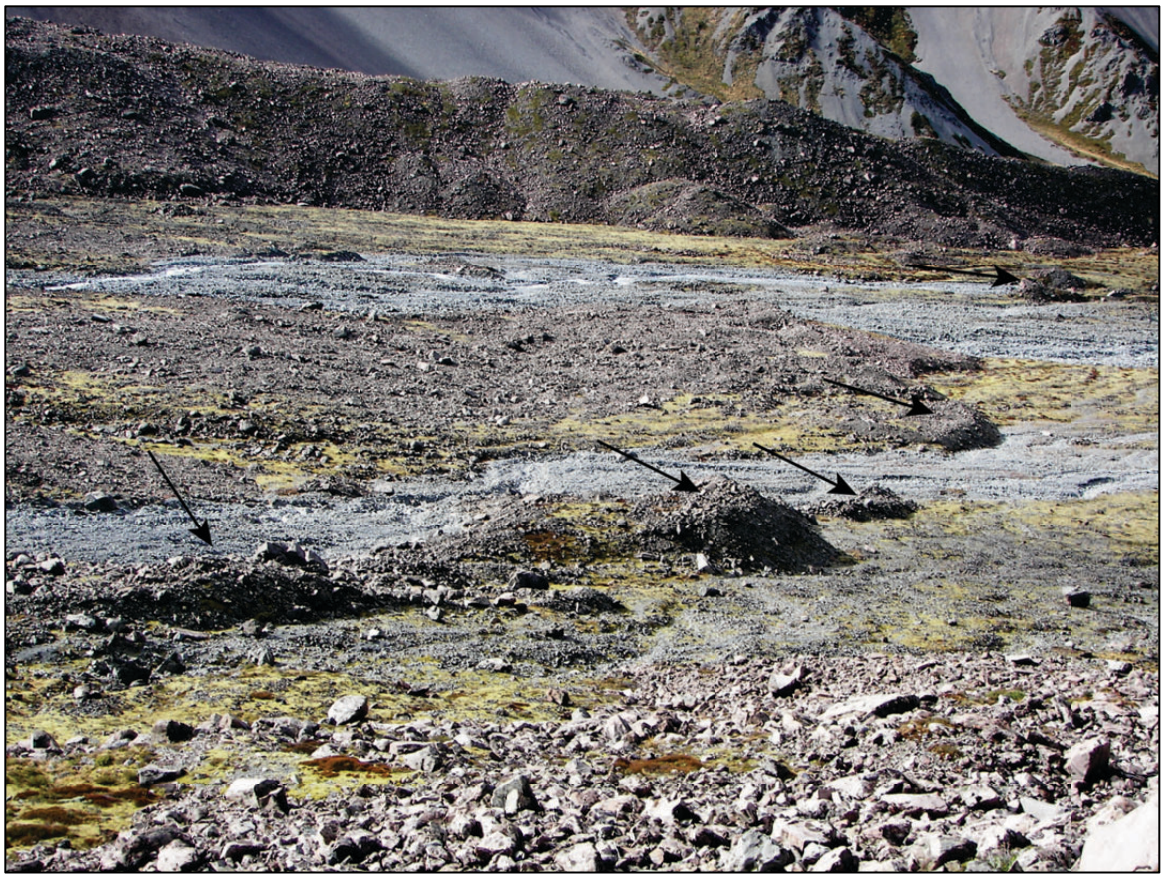

Figure S10. Photograph, vantage east, of the discontinuous A2 ridge on the valley bottom. Ridge segments are arrowed. Glacier flow was from the left. Imagery date: April, AD2006.

A subsequent minor readvance or stillstand deposited a small terminal moraine ridge segment (A1) in the middle of the valley floor, about 0.46 km inboard of the A2 ridge (Figs. S2 and S4). Incision by the Cameron River has removed most of the terminal ridge; only a 130 m-long bouldery segment remains superimposed on a slightly raised patch of ground moraine. The left-lateral continuation of the A1 moraine ridge can be traced to the northeast, across an eastern channel of the Cameron River. The A1 left-lateral moraine segment is 0.21 km long, and grades up to the north along the base of the A2 ice-contact slope. At its northern end the A1 left-lateral moraine merges with A2 and A4 to form a composite left-lateral ridge mentioned above.

The valley-floor landscape inboard of the A1 ridge is dominated by recessional ground moraine that has been dissected by migrating channels of the Cameron River. The modern (i.e., AD2006) Cameron Glacier terminus lies 1.33 km up-valley of A1. In addition, Burrows[7] documented terminal positions of the Cameron Glacier in AD1964 and AD1989, when the ice margin lay 0.85 and 0.35 km, respectively, outboard of the AD2006 terminus.

4.0 ^{10}Be surface-exposure dating

4.1 Field methods

We followed the field procedures described in detail in Schaefer et al.[18], Putnam et al.[14,19], and Kaplan et al.[20]. In the interest of constructing a precise ^{10}Be surface-exposure moraine chronology that accurately reflects past glacier behavior, we sampled boulders embedded in, or resting in stable positions on, morphologically distinct mapped moraine-ridge crests (Fig. S11) with intact soil profiles and native vegetation cover. We chose boulders with flat or gently rounded top surfaces with low surface dip, and avoided sampling from fractured, pitted, moss-covered, or spalled sectors on boulder surfaces.

Excluded from the sampling program were boulders less than ~50 cm tall, and any boulders located near disturbed or degraded regions such as slumps, river cuts, or places in which introduced grazing mammals have initiated severe soil erosion. We also avoided sampling in potentially unstable locations such as steep slopes and rockfall run-out zones near cliff faces or talus slopes.

For each selected sample we measured boulder dimensions and boulder height-above-ground in at least four places around the boulder. We measured the heights of as many as ten different quartz veins near the sampled surface, and took note of general weathering rind thickness and lichen cover. Following the suggestions of Winkler and Matthews[21], on that part of the moraine complex lying west of Cameron River, we measured Schmidt hammer rebound values (Q-values) in at least ten different locations on the greywacke matrix near the chosen sample site on each sampled boulder. We measured Q-values using a certified anvil-calibrated digital 'SilverSchmidt' Concrete Test Hammer. Prior to each impact we made sure to secure the hammer in a position perpendicular to the boulder surface. The hammer was triggered with elbows firmly anchored on the boulder in order to avoid errant impacts. We avoided testing surfaces containing clearly loose fragments, surface fractures, dilatant sub-surface fractures (indicated by sounding a hollow 'thunk' when struck with a chisel), ponded water, or moss/lichen cover.

Figure S11. Examples of boulders sampled for ^{10}Be surface-exposure dating. Top left. Photograph, vantage northwest, of boulder resting on A2 moraine. Top right. Photograph, vantage east, of boulder on crest of A4/A3 moraine ridge. Middle left. Photograph, vantage south, of boulder embedded in B2 moraine ridge crest. Middle right. Photograph, vantage north, of boulder embedded in B2 moraine ridge. Bottom left. Photograph, vantage north, of boulder embedded in B6 moraine ridge. Bottom right. Photograph, vantage south, of boulder resting on C2 moraine ridge. Imagery date: April-May, AD2006.

We used compass and clinometer to map azimuthal elevations of the horizon at each sample site. These measurements were later used to model and correct for the effects of topographic shielding on ^{10}Be ages. All boulders and sample surfaces were photographed from several different angles, and two different operators drew each boulder in the context of the surrounding landscape. Global positioning system (GPS) locations (latitude, longitude, and height above mean sea level) for all boulders were collected using a Trimble ProXH GPS receiver. All GPS data were subsequently differentially corrected against data collected at the Mount John Observatory base station, located 70 km southwest of the Cameron Glacier moraines (MTJO; latitude: -43.985706, longitude: 170.46493, height above ellipsoid: 1043.660 m; height above mean sea level relative to the tide-gauge datum at Lyttelton, New Zealand: 1037.46 m). Latitudes and longitudes are reported relative to the WGS 1984 datum. Elevations are referenced to elevation above mean sea level based on the Lyttelton tide-gauge datum. Horizontal and vertical uncertainties in our sample locations range from 0.2 to 0.4 m and 0.2 to 0.6 m (1σ), respectively.

Samples were collected by hammer and chisel and/or the drill-and-blast method of Kelly[22]. We aimed for broad, thin (<4 cm thick) samples. Only rock fragments retaining the original rock surface were collected. All samples were shipped to the Cosmogenic Nuclide Laboratory at the Lamont-Doherty Earth Observatory for rock preparation and Be extraction.

4.2 Laboratory methods

At the LDEO Cosmogenic Nuclide Laboratory, for each sample we measured the thickness of each rock fragment using mm-precision calipers, and then calculated an average mass-weighted thickness for the sample. We made drawings of each rock fragment, recorded all measured thicknesses, and measured rock-fragment masses. We then crushed, pulverized, and sieved fragments in each sample. The 125-710 μm fraction was isolated for chemical leaching. All other grain sizes were stored as archive material.

We processed all samples for Be extraction following the LDEO Cosmogenic Nuclide Laboratory ^{10}Be laboratory protocol available online at: http://www.ldeo.columbia.edu/tcn. Detailed methods pertinent to accurate measurement of small ^{10}Be concentrations in rocks are presented in Schaefer et al.[18]. Be extracts from each sample were sent to the Lawrence-Livermore National Laboratory Center for Accelerator Mass Spectrometry (LLNL CAMS) for ^{10}Be/^{9}Be measurement. With the exception of one sample, all measurements were made relative to the 07KNSTD3110 standard [^{10}Be/^{9}Be = 2.85 x 10^{-12}; ref. 23]. Sample CG-06-41 was measured relative to the KNSTD3110 standard, and subsequently normalized to 07KNSTD3110 by applying a correction factor of 0.9042 (ref. 23). All measured ratios were corrected for residual boron contamination (<1%). Ratios were then converted to numbers of ^{10}Be atoms (in atoms) and subsequently corrected for procedural ^{10}Be contamination by subtracting the number of ^{10}Be atoms measured in procedural blanks from numbers of ^{10}Be atoms measured in respective sample concentrations. Samples were then converted to ^{10}Be concentrations (in atoms g^{-1}). Blank corrections were typically <1% for samples with ^{10}Be concentrations >10,000 atoms g^{-1}, and ranged from 3 to 6% for samples with

concentrations <10,000 atoms g^{-1}. We propagated absolute blank errors in quadrature with attendant AMS analytical uncertainties. ^{10}Be data are given in Table S1.

4.3 ^{10}Be surface-exposure ages

We calculated ^{10}Be surface-exposure ages from corrected ^{10}Be concentrations using the precise locally determined ^{10}Be production-rate of Putnam et al.[19]. Production rates were scaled from sea level and high latitude to sample locations using the protocols of Lal[24]/Stone[25] ('St'), Lifton et al.[26,27] ('Li'), Dunai[28] ('Du'), Desilets[29] ('De'), as well as a time-dependent version of the Lal[24]/Stone[25] altitudinal scaling method that incorporates a high-resolution version of the Lifton et al.[27] geomagnetic model[19] ('Lm'). Because New Zealand is located at southern middle latitudes and is influenced primarily by the geomagnetic dipole, time-dependent effects of geomagnetic change on in-situ ^{10}Be production over the course of the Holocene are likely to be small and reliably captured by the Lifton et al.[27] geomagnetic model. Close agreement among empirically derived ^{10}Be production rates integrated over Holocene time at middle to high-latitude sites in South America[30], Norway[31], and Greenland[32] imply that New Zealand has not been uniquely influenced by prominent non-dipole geomagnetic excursions over the last ~10,000 yrs or so. Furthermore, ^{10}Be ages determined from late-Holocene moraines in the Southern Alps show good agreement with independent age controls (on the basis of direct ^{14}C control or historical documentation) when ^{10}Be ages are calculated using the Putnam et al.[19] calibration with the Lm scaling scheme (for example, see section 5.1 comparison between ^{14}C-^{10}Be ages on moraine A4/A3, and see Schaefer et al.[18] for similar examples from the Aoraki/Mount Cook region).

To expedite comparison with calendar-year converted ^{14}C ages, we referenced all ^{10}Be ages to the year AD1950 by subtracting 56 and 57 yrs from samples collected in AD2006 and AD2007, respectively. All calculated ^{10}Be surface-exposure ages, referenced to AD1950, are listed for each scaling protocol in Table S2. All scaling schemes yield agreement to less than 1% for ages older than a few thousand years (i.e., <100 yrs for samples ~10,000 yrs old), and agreement of 2-3% for ages younger than 600 yrs (i.e., <30 yrs for a ~500-yr old sample, and <10 yrs for a ~100-200-yr old sample). We discuss ages calculated using the Lm scaling scheme because this method seems to produce ^{10}Be ages for landforms that agree best with direct radiocarbon age control for those same landforms[19]. However, given the extremely close agreement among ages calculated using different scaling protocols, choosing a different scaling scheme would not alter any of our conclusions.

We corrected each sample for the effects of topographic shielding using the program written by G. Balco available online at the CRONUS-Earth website: http://hess.ess.washington.edu/math/. Shielding corrections were typically less than 3%. Persistent, deep, and dense snow cover has been suggested to shield and hence reduce production of cosmogenic nuclides in surface rocks. However, winter snow does not typically persist for periods longer than weeks at altitudes <1500 m in the Southern Alps. Furthermore, winds tend to remove snow from salient moraine ridge crests and boulder tops. For these reasons, we do not apply any corrections for snow cover.

Landscape uplift also impacts *in situ* cosmogenic-nuclide production. Uplift of a land surface toward progressively higher altitudes, and hence into progressively lower atmospheric pressures, exposes rock surfaces to increasing cosmic-ray fluxes, therefore

increasing the *in situ* production of cosmogenic nuclides. In this regard, the Cameron Glacier moraine system is located ~36 km southeast of the Alpine Fault, in a region where average long-term uplift rates are estimated to be ~1.6 mm yr^{-1} (ref. 19). The rate of vertical landscape rise at the Cameron Glacier is likely to be similar to that at the Macaulay valley production-rate calibration site, which lies ~38 km southeast of the Alpine Fault trace. Because production rates calculated at the Macaulay site were not corrected for the effects of landscape uplift, and because uplift rates are judged to be similar between the Macaulay site and the Cameron moraine site, any such effects of landscape uplift (if any) have already been factored into the production-rate determination and therefore require no additional correction.

Erosion of boulder surfaces can also affect ^{10}Be surface-exposure ages by removing accumulated nuclides at the surface, and hence lowering the 'apparent' ^{10}Be age with respect to the true exposure age. In this regard, the greywacke sandstone of the Torlesse Composite Terrance is relatively resistant to granular disintegration due to the interlocking nature of quartz crystals in the rock matrix[13]. Quartz-vein heights can be used to estimate the amount of granular disintegration on moraine boulders in the Cameron valley. We found that quartz vein heights were flush (i.e., within the limitations of field caliper measurement, about <0.5 mm) with adjacent sandstone-lithology surfaces on boulders first exposed between 0 and 520 yrs ago (based on ^{10}Be ages uncorrected for erosion), implying an erosion rate of less than 1 mm per thousand years (i.e, within measurement limitations). The largest quartz-vein heights identified among all boulders sampled for ^{10}Be surface-exposure dating were ~4-5 mm for boulders exposed ~10,000 yrs ago, implying an erosion rate of 0.5 mm per thousand yrs. Our quartz-vein-height

results are similar to those obtained from independently ^{10}Be-dated deposits in the Ben Ohau Range[13,20], ~100 km southwest of Cameron valley. For example, Birkeland obtained an average quartz-vein height of 4.30 ± 1.32 mm for the 'Ferintosh' moraines in various valleys of the Ben Ohau Range. Kaplan et al.[20] subsequently obtained ^{10}Be ages from the 'Ferintosh' moraines described by Birkeland[13] at the head of the Irishman Stream valley to between 12,900 and 12,000 yrs ago, indicating an erosion rate of ~0.4 mm per thousand years. Such low erosion rates would change ^{10}Be ages by less than ~0.5% (i.e., well within the analytical uncertainty). For these reasons, we do not include a correction for erosion in ^{10}Be surface-exposure-age calculations.

5.0 Chronology

5.1 ^{10}Be surface-exposure chronology for the Cameron Glacier moraines

In almost all cases, multiple ^{10}Be surface-exposure ages determined from single moraine crests showed excellent internal consistency and formed approximately normal distributions (Table S3, Fig. S12). Experimentally determined χ^2 values for moraine ridges C3, B6, B4, B3, and B2, were less than values expected for normal distribution at 95% confidence (Table S3). Such low χ^2 values imply that all sample variability can be explained by analytical uncertainty, and that post-depositional geological influences that some workers have suggested may impact surface-exposure ages randomly (such as surface disintegration, spalling, boulder rotation, moraine degradation, inheritance from prior exposure, snow cover, etc.) have been insignificant[33,34]. In such distributions of

approximately normal shape and where outliers are absent, we assign the arithmetic mean and standard deviation (i.e., ± 1σ) as the age of the moraine.

In cases where χ^2 values are higher than expected for normal distributions at 95% confidence, or in cases where visual inspection of cumulative probability plots leads to suspicion of statistical-outlier samples, we follow Dunai[35] and test whether suspect ages are indeed statistically different from the rest. For this purpose we implement the Chauvenet criterion[34] and the Grubbs test[36] outlier rejection methods, assessed iteratively at the 95% confidence interval. In addition, we employ the classic geological principle of stratigraphic superposition (in this case morphostratigraphic superposition) in order to assess whether a sample age is stratigraphically incompatible with ages of moraines located inboard or outboard.

We identified and rejected one outlying age (CG-06-39; 8,650 ± 350 yrs) from moraine C2 on the basis of the Chauvenet criterion, and on the basis of the sample age being too young in comparison to the age of the inboard B6 moraine (9140 ± 140 yrs). In addition, we identified and rejected one outlier from A5 (CG-06-19; 1700 ± 70 yrs) based on the Chauvenet criterion[34] and Grubbs test[36], assessed at 95% confidence. In both cases, removal of one outlier each from the C2 and A5 moraine age distributions resulted in an approximately normal cumulative probability curve and experimental χ^2 values less than those expected for normal distributions of those sizes at the 95% confidence level.

In the case of moraine A4, we removed three suspect ages: CG-06-09 (1140 ± 60 yrs), CG-06-10 (770 ± 30 yrs), and CG-06-13 (3890 ± 100 yrs). All three ages are outliers according to the Chauvenet criterion[34] and Grubbs test[36]. Finally, we rejected one sample (CG-06-02; 407 ± 18 yrs) from the A2 moraine age on the basis of the

Chauvenet criterion[34]. In both cases, the A4 and A2 data sets still formed non-normal distributions even after rejection of outliers with χ^2 values larger than those expected. Thus we do not exclude the possibility that prior exposure may have influenced the moraine A4 and A2 ages. We also do not exclude the possibility for A4 that the younger shoulder apparent on the cumulative probability curve represents a second advance into the A4/A3 moraine. Burrows[9] mapped the A4/A3 ridge as a composite ridge, and noted a bimodal lichen distribution. Thus, we consider it possible that a secondary mode, just barely distinguishable from the dominant mode, represents a secondary advance that culminated shortly after ~500 yrs ago (i.e., ~AD1450). Given this possibility, but with no striking geomorphological evidence for a younger moraine superimposed on A4, we take the arithmetic mean and standard deviation of the full distribution. In this case the error bars encompass both modes. We note that a minimum-limiting ^{14}C date (527 ± 36 cal. yrs; N.Z. 687) on this moraine ridge, described in section 3.4.3 above, is consistent with the arithmetic mean calculated here.

All assigned moraine ages, with outliers removed, are given in Table S4 and Fig. S13. These ages form the underlying geochronological framework for the Cameron Glacier snowline and temperature reconstructions, described below.

As described above in section 4, because we use a local ^{10}Be production-rate derived from an early Holocene debris-flow deposit in the Macaulay valley (~1000 m a.s.l.), systematic scaling errors are negligible. Another systematic uncertainty that must be considered is the production-rate uncertainty. Table S4 shows the systematic age offsets that result when moraine ages are calculated using the ±2.2% production-rate uncertainty limits. Choosing a different production rate (such as the upper or lower error

limit) results in a systematic shift of the chronology. By using the upper or lower error bound of the production-rate uncertainty to calculate ^{10}Be ages, the oldest moraine ages (e.g., C3 and C2) shift by about ± 200 yrs and the youngest moraine ages (e.g., A4 and A2) shift by about ± 10 yrs (Table S4).

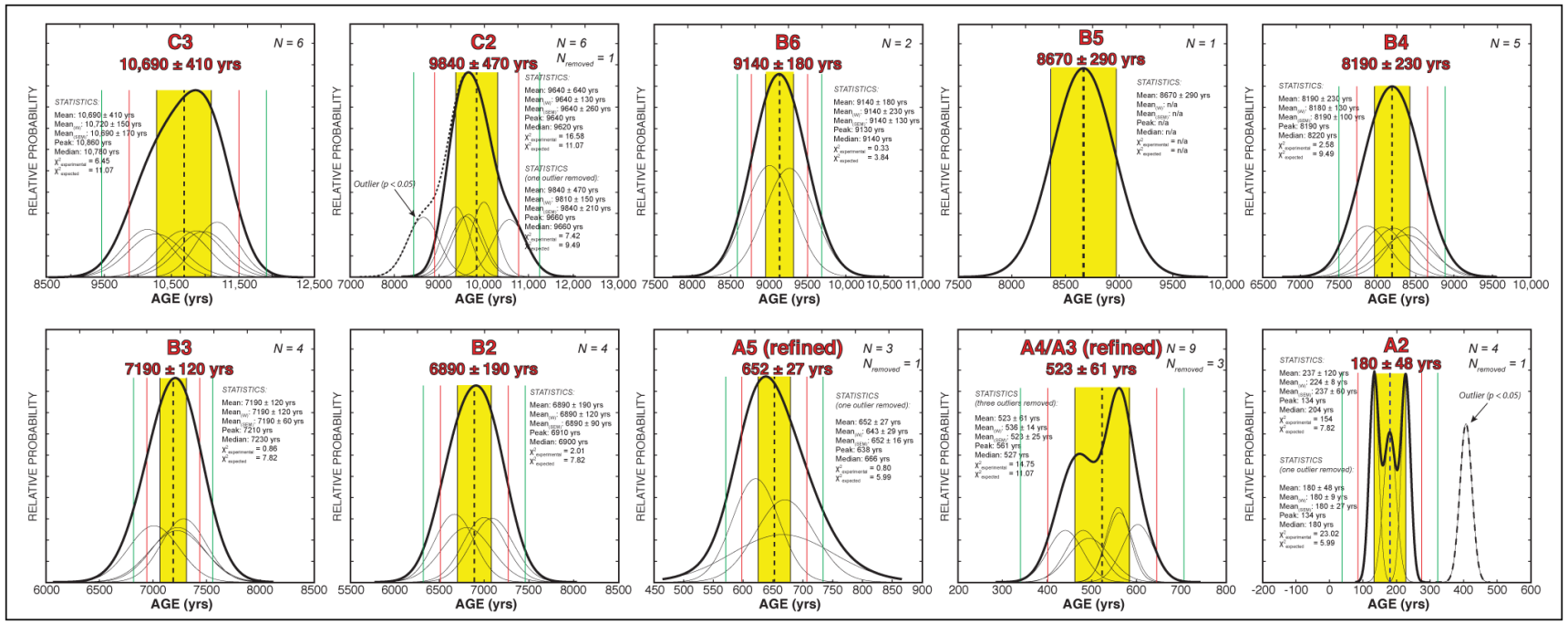

Figure S12. Relative probability distributions of ^{10}Be exposure ages grouped by moraine ridge. Thin black lines are individual age probabilities (1σ), and bold lines are the cumulative probability of the distribution. Numbers in bold red font are the arithmetic mean and standard deviation (1σ) of the population (yellow band), interpreted to represent the time since moraine formation was completed. Additional statistics are included as insets. Vertical lines are 1σ (black), 2σ (red), and 3σ intervals. Panels showing moraine A5 and A4/3 distributions are scaled such that much older 'outlier' ages are not shown (labeled as 'refined').

5.2 Determining the age of moraine A1 by combining ^{10}Be surface-exposure dating and lichenometry

We did not attempt to obtain ^{10}Be ages from the innermost A1 ridge of the Cameron Glacier moraine complex. Its location inboard of the AD1864 glacier terminus illustrated by Haast[6] implies that the A1 ridge must be younger than AD1864. Although we do not have ^{10}Be data for the A1 ridge, two attempts[7,9] have been made to define the age of the A1 moraine using lichenometry. Burrows[9] obtained an age of AD1930 using a ^{14}C-based calibration curve for *R. geographicum*. In contrast, Burrows et al.[7] calculated a *R. geographicum* age of AD1820, derived from a revised lichen-diameter calibration from Aoraki/Mount Cook National Park, based on weathering-rind thickness estimates of moraine ages. We consider that the age of AD1820 determined by Burrows et al.[7] can not be correct because the ice margin is known to have been down-valley of the A1 position in AD1864. Here, in a third attempt to derive an age for moraine A1, we combined Burrows' lichen diameter data with ^{10}Be surface-exposure dating. We used the arithmetic mean ^{10}Be moraine ages for A4 and A5 (referenced to AD1950), as well as the historical age of AD1864 for the A2 moraine, to produce a local calibration curve for *R. geographicum* based on maximum lichen thalli measured by Burrows[9] and Burrows et al.[7] for the last ~650 yrs. Fig. S13 shows the ^{10}Be-based *R. geographicum* calibration curve.

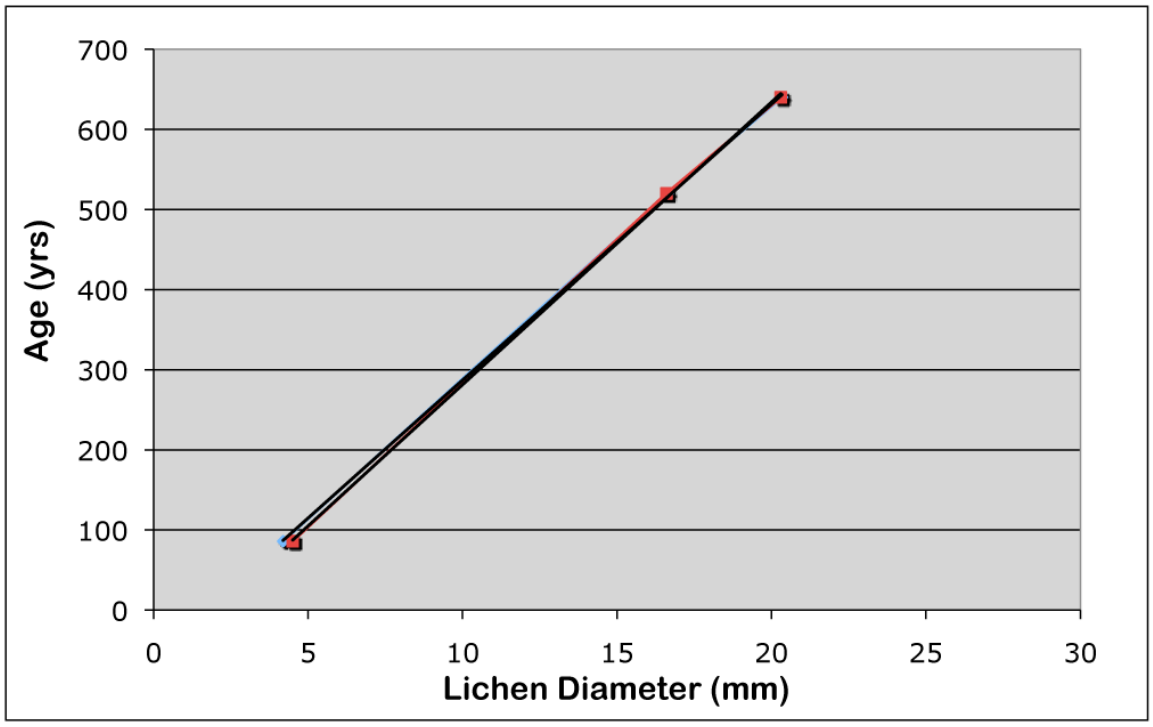

Figure S13. Lichen growth curves for the last ca. 700 yrs constructed using lichen diameters measured by Burrows[9] (red squares) and Burrows et al.[7] (blue diamonds) and the ^{10}Be surface-exposure age for the same landforms. Age of 0 yrs = AD1950. Black lines are linear regressions.

Although the ^{10}Be-based lichen curve contains only three calibration points, all points are highly linearly correlated ($r^2 = 0.99$). We plotted both data sets reported by Burrows[9] in AD1975 and by Burrows et al.[7] in AD1990 and both calibration curves demonstrate close consistency and are virtually indistinguishable. The best-fit linear trends relating *R. geographicum* thalli to age (in yrs BP) for the Burrows[9] and Burrows et al.[7] data sets are described by Equations (S1) and (S2), respectively.

Equation S1: $y = 34.444x - 57.359$

Equation S2: $y = 35.263x - 71.294$

Where y, the dependent variable, is age, and x, the independent variable, is lichen diameter. Burrows[9] and Burrows et al.[7] measured lichen diameters for the A1 moraine of 2.18 cm and 3.2 cm, respectively. Calculation of respective lichen ages using each calibration yields ages of AD1930 and AD1910, respectively. The y-intercept on the first calibration curve (Equation B.1), based on the data of Burrows[9], would imply a lichen colonization time of ~57 yrs. The y-intercept on the second calibration curve (Equation B.2), based on the data of Burrows et al.[7], would imply a lichen colonization time of 71 yrs. Observed colonization periods for *R. geographicum* are on the order of ~40 yrs or faster for the central Southern Alps[37]. Furthermore, many glaciers of the Southern Alps, including the Franz Josef[10,38-40], Fox[40], and Stocking[10,38] glaciers, were documented just inboard of AD1860s positions ca. AD1930. Given these two observations, we assign an age of AD1930 (i.e., 20 yrs before AD1950) to moraine A1 on the basis of the original lichenometry data set of Burrows[9] calibrated to the ^{10}Be chronology presented here.

Finally, we use the calibration based on the original Burrows' data (i.e., Equation (B.1)) to calculate an age for a small moraine remnant located between A4/A3 and A2, named 'A2b' by Burrows[9]. Burrows determined a maximum *R. geographicum* diameter of 6.35 cm from this moraine ridge. Conversion of this lichen diameter yields a lichenometric age of AD1789 (i.e., 161 yrs before AD1950), which we here assign to A2b.

5.3 Developing a Southern Alps composite glacier chronology for the Holocene

5.3.1 Geomorphologic setting of Cameron Glacier and Mueller, Hooker, and Tasman glaciers

There is a distinct geomorphologic difference between Cameron Glacier and the Mueller, Hooker and Tasman glaciers. At Cameron Glacier the valley has a relatively steep but uniform gradient, a narrow, largely single-thread, outwash channel that cuts cleanly through the moraine belts, and comparatively little accumulation of fluvial sediment in the moraine belts (Fig. S2). In contrast, the Aoraki/Mt. Cook glacier systems are larger, have lower gradients, and adjoin an aggrading sandur that links to a prograding fluvio-deltaic system that is infilling the Last Glaciation glacier trough occupied by Lake Pukaki. As a result, the entire Holocene moraine sequence of the Cameron Glacier is well expressed with little post-depositional modification, whereas at the main valley glaciers of the Aoraki/Mt Cook area, the negligible record of early Holocene moraines and patchy preservation of mid-Holocene moraines most likely reflects destruction by widespread outwash stream erosion or burial by outwash aggradation.

5.3.2 Composite chronology

Comparison of the Cameron Glacier moraine chronology with the updated ^{10}Be surface-exposure moraine chronology of Schaefer *et al.*[18] for Mueller, Hooker, and Tasman glaciers of Aoraki/Mount Cook National Park (Table S5) reveals distinct similarities and differences (Fig. S14). A notable similarity among the Cameron, Mueller, and Tasman glaciers is the existence of ~6700 yr-old moraines in each valley

located outboard of late Holocene moraines. The combined age of the outboard 'Little Hump' (Tasman) and 'Foliage Hill' (Mueller) moraines is 6740 ± 160 yrs, whereas the age of the Cameron Glacier B2 ridge is 6890 ± 190 yrs (Fig. S15a). These moraine ages agree within respective 1σ analytical uncertainty. At both the Mueller and Cameron glaciers, prominent ~500- to ~600-yr-old moraines lie inboard of the equivalent ~6700-yr moraines. At Mueller Glacier that moraine has an age of 563 ± 82 yrs, while at Cameron Glacier are the 652 ± 27 yr A5 moraine, and the 523 ± 61 yr A4/A3 composite moraine. These young moraines are at equivalent morphostratigraphic positions in the Mueller and Cameron valleys, and ^{10}Be ages afford arithmetic-mean ages that overlap within 1σ analytical uncertainty (Fig. S15b). However, the Mueller Glacier moraine complex differs in having a localized remnant of stacked moraines ranging in age from ~2300 to ~3400 yrs, slightly outboard of the ~560-yr moraine. These stacked moraines were not overwhelmed by the 560-yr advance because they form a barrier (called 'White Horse Hill') that in part impeded the glacier during the 560-yr advance. A similar barrier exists at Tasman Glacier.

A blocking moraine barrier, such as White Horse Hill at Mueller Glacier, does not occur at the Cameron Glacier, and thus no such 'protected' moraines are preserved morphologically. However, four anomalously old boulders dated from the A5 and A4/A3 (i.e., ~650 and ~520-yr) moraine invite at least two possible interpretations. One is that the advances to the A5 and A4/A3 moraines may have recycled boulders from older moraine surfaces located slightly inboard of these moraines. Another explanation is that these moraine ridges are more composite in age than we realize, and possibly include the emergent tips of older remnant ridges only just overwhelmed, and not eroded, by these

young advances. At all events, if the numerous mid- to late Holocene glacier fluctuations recorded by moraines at the Mueller, Hooker, and Tasman glaciers also occurred at the Cameron Glacier, it is clear from the dating presented here that none of those fluctuations was more extensive than the ~650-yr and ~520-yr advances of the Cameron Glacier.

Here we make use of the robust overlap between 'non-protected' moraine ridges at Cameron, Mueller, and Tasman glaciers, and combine the chronologies. We assume that the 'protected' moraines dated at Mueller Glacier represent advances to positions very close to the 560-yr moraine limit. We then assume that those moraines correspond to snowlines of similar elevation as the snowline reconstructed for the 523 ± 61-yr moraine at Cameron Glacier, which we assume is related to the same climate change that triggered the Mueller Glacier advance to its 560-yr position (Table S5). We make the same assumption for the Tasman Glacier, and assume that 'protected' moraines correspond to snowlines similar to, or only slightly higher than, the snowline elevation reconstructed for the 520-yr A4/A3 moraine (described below). In this way we are able to patch together these chronologies into a provisional composite chronology of Southern Alps glacier fluctuations during the Holocene, from which glacier geometry can be reconstructed and associated snowline estimated, and from which palaeo-temperatures may be inferred. In the next section we describe and discuss snowline and temperature reconstructions.

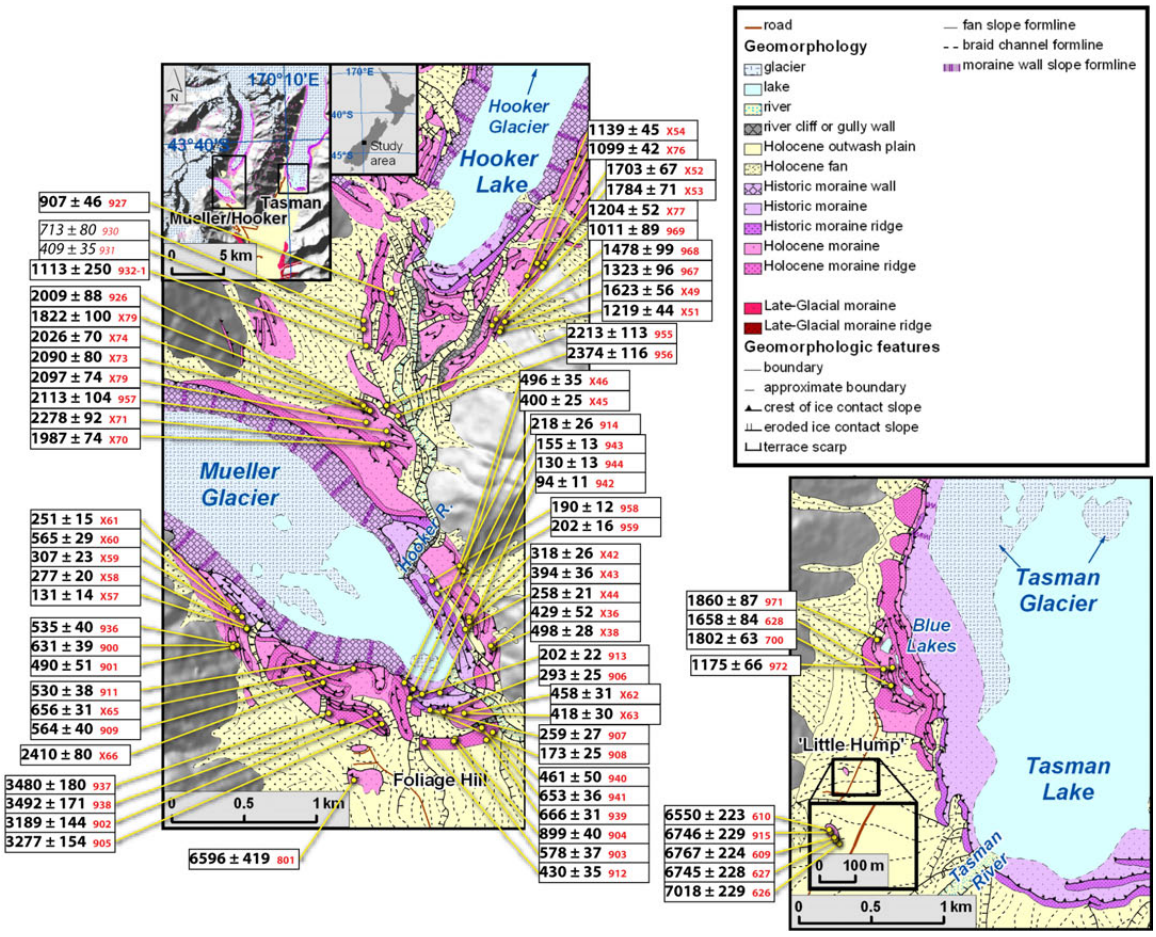

Figure S14. Glacial geomorphologic maps of the Mueller, Hooker, and Tasman glacier moraine sets of the Aoraki/Mount Cook region (updated from Schaefer et al.[18]). Geomorphologic units and boundaries are described in legend, inset. ^{10}Be surface-exposure ages are given in white boxes, and yellow dots denote sample locations. Red text refers to sample ID. All ages have been recalculated using the New Zealand ^{10}Be production rate[19] and the 'Lm' scaling protocol.

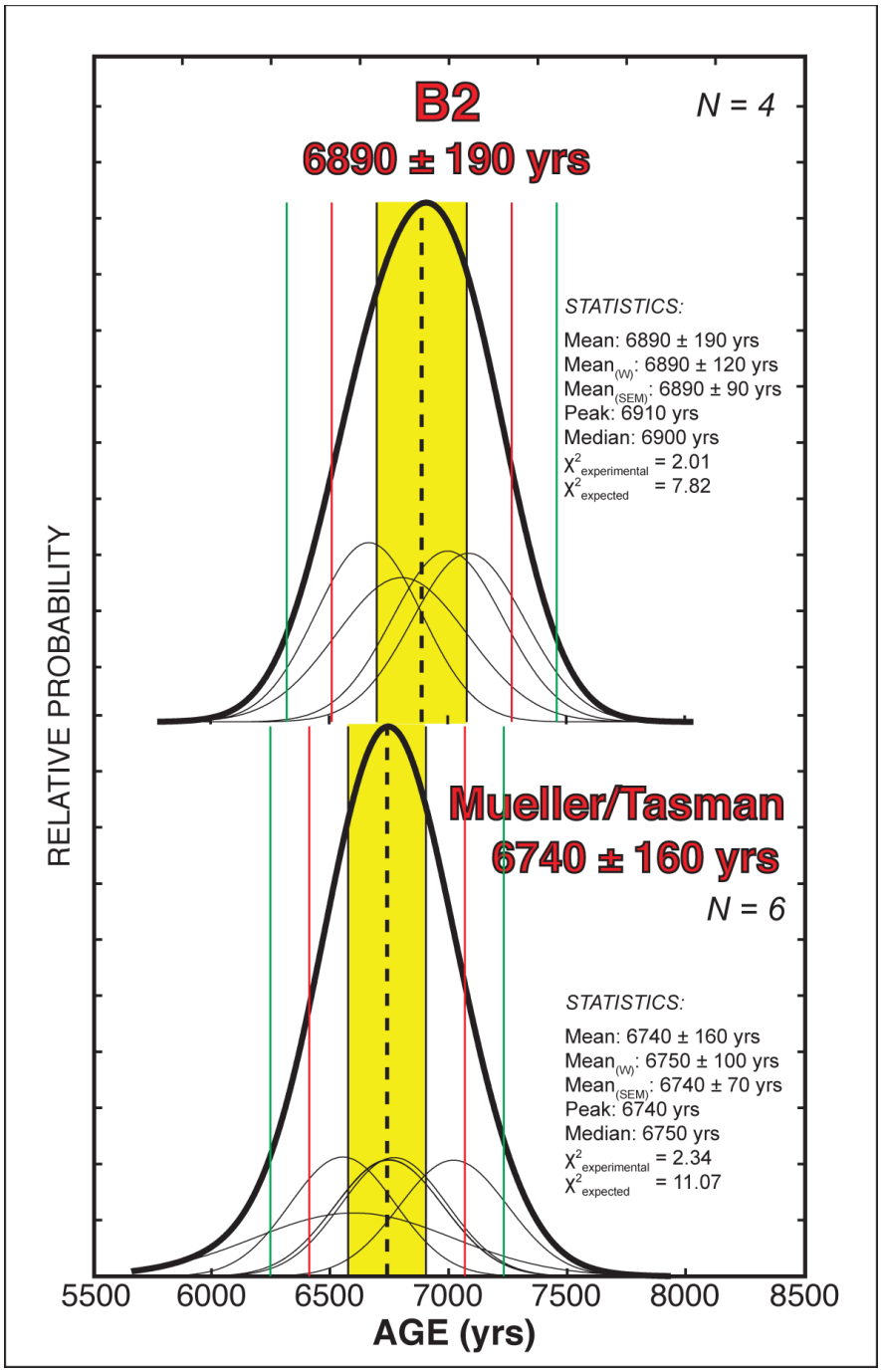

Figure S15a. Comparison of probability distribution plots for the B2 and Mueller/Tasman outboard moraines. All ages have been recalculated using the New Zealand ^{10}Be production rate[19] and the 'Lm' scaling protocol. Thin black lines are individual age probabilities (1σ), and bold lines are the cumulative probability of the distribution. Numbers in bold red font are the arithmetic mean and standard deviation (1σ) of the population (yellow band), interpreted to represent the time since moraine formation was completed. Vertical lines are 1σ (black), 2σ (red), and 3σ intervals. Additional statistics are included as insets.

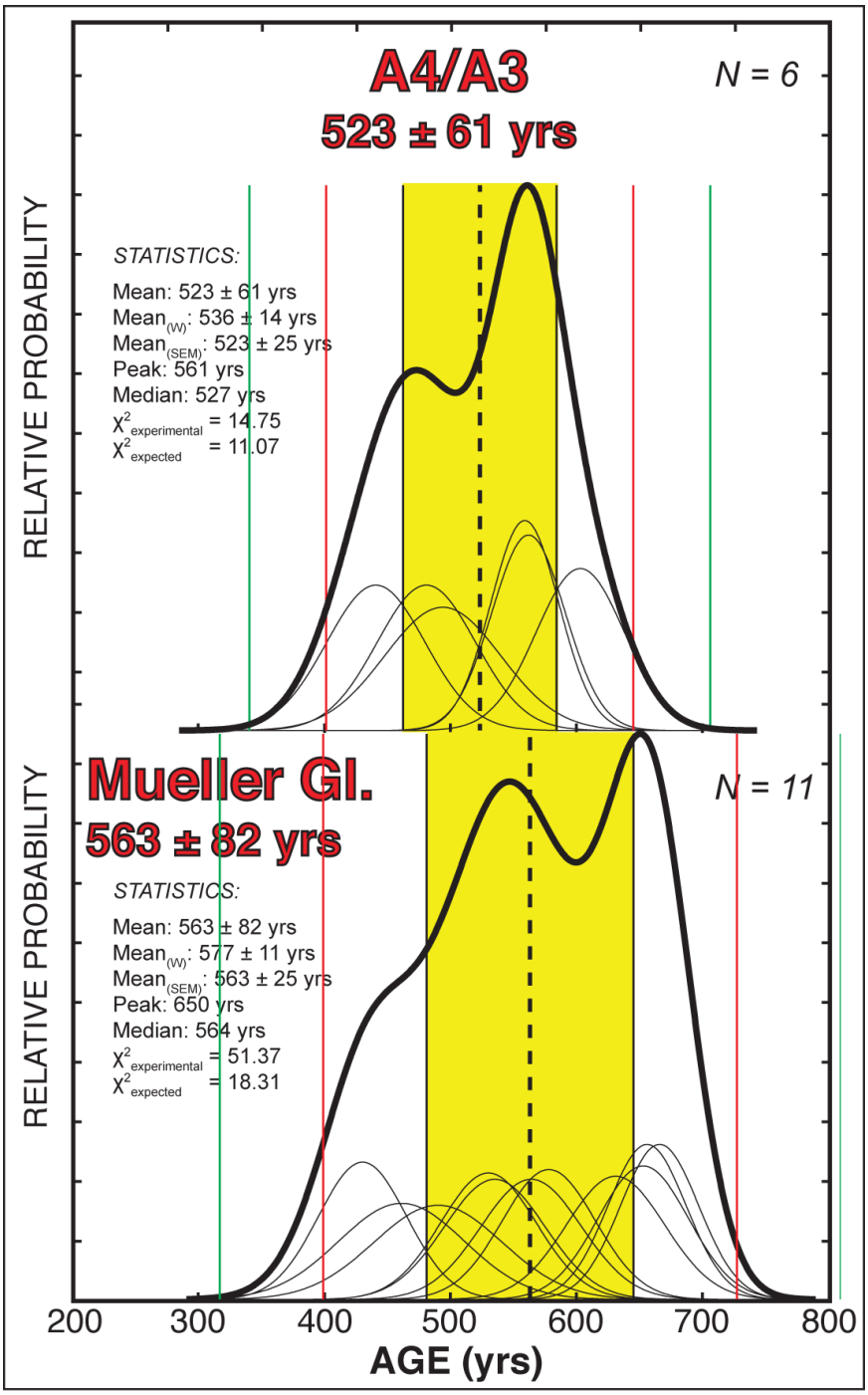

Figure S15b. Comparison of probability distribution plots for A4/A3 and the prominent '550-yr' moraine at Mueller Glacier. All ages have been recalculated using the New Zealand ^{10}Be production rate[19] and the 'Lm' scaling protocol. Thin black lines are individual age probabilities (1σ), and bold lines are the cumulative probability of the distribution. Numbers in bold red font are the arithmetic mean and standard deviation (1σ) of the population (yellow band), interpreted to represent the time since moraine formation was completed. Vertical lines are 1σ (black), 2σ (red), and 3σ intervals. Additional statistics are included as insets.

6.0 Snowline and temperature reconstructions

The well-preserved Cameron Glacier terminal moraines provide close constraints on the former downstream extents of the Cameron Glacier, whereas upstream ice limits are well defined by the catchment head. The Cameron Glacier moraine complex is therefore well suited to robust snowline reconstruction using the accumulation-area ratio (AAR) method[41]. We generated snowlines using the 'larger-volume ice model' version of the AAR method employed by Kaplan et al.[20]. This particular version of the AAR method assumes that the upstream glacier margin extended to the catchment head, and thus accounts for ice and snow inputs from the steep headwalls. The 'smaller-volume ice model', also employed by Kaplan et al.[20], extends the upstream glacier margin to the bases of bluffs around the perimeter of the catchment headwall. Because the upper limit of the glacier at the headwall remains relatively constant during glacier expansions and contractions, we chose to use the larger-volume ice model because the catchment perimeter, defined by arêtes and peaks, is easier to hold constant while performing multiple snowline reconstructions for former glacier geometries of different size. The amount of area added to the 'smaller-volume ice model' accumulation area is a small proportion of the cumulative glacier area (~2-4%), and therefore has minimal effect on resulting snowline estimations[20].

We reconstructed the Cameron Glacier for 4 moraine limits, W2, C2, A4/A3, and A2 (Fig. S16), defining the glacier surface with topographic contours at 100-m intervals. Cumulative glacier area was determined for each 100-m contour using computer-based mapping tools in ArcGIS version 9.1. We derived snowlines from cumulative area-

versus-altitude plots for each glacier reconstruction (Fig. S16), based on the global average accumulation-area to ablation-area ratio (AAR) of 2:1 or 0.67/0.33. Chinn et al.[42] showed that this AAR value is broadly applicable to New Zealand glaciers. Because our glacier topographic reconstructions are based on the photogrammetrically mapped 20-m topographic contours, we follow Kaplan et al.[20] and assign a minimum systematic uncertainty of ±20 m to snowline values. However, because we reconstructed snowlines using 100-m contours, a more conservative systematic uncertainty for our overall reconstruction is plus or minus half a contour interval, i.e. ±50 m. These uncertainties are tempered by a robust assumption that any particular end moraine ridge relates to a glacier snowline that was lower than the glacier snowline that produced the next adjacent, younger, moraine up-valley.

Wildman

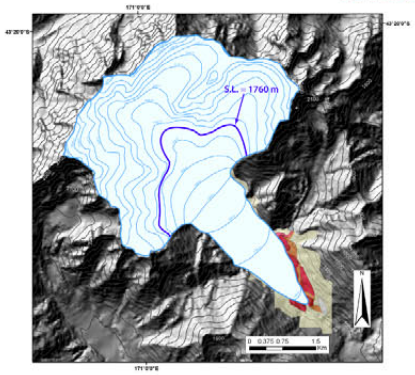

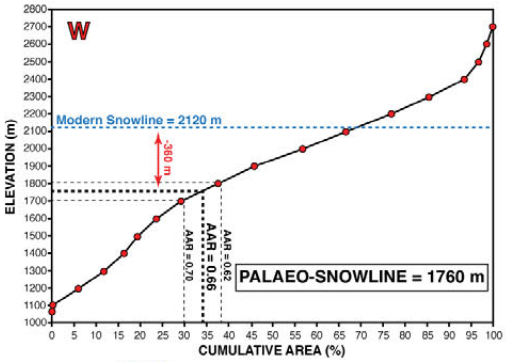

Outer Marquee C2

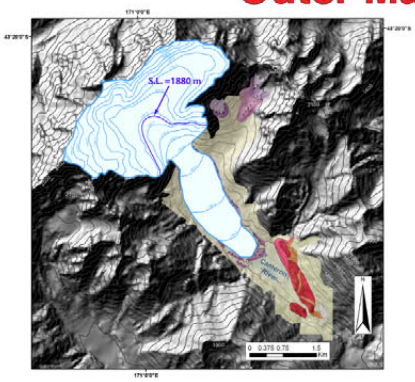

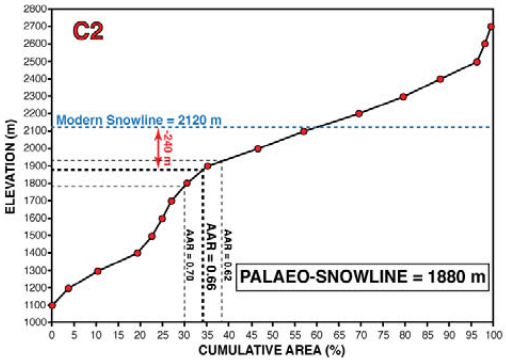

Arrowsmith A4/A3

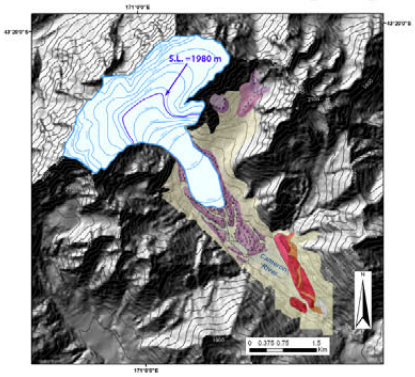

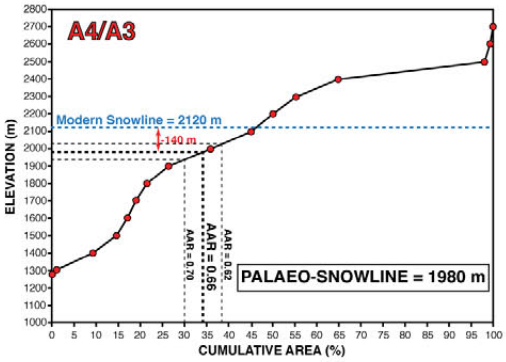

Arrowsmith A2

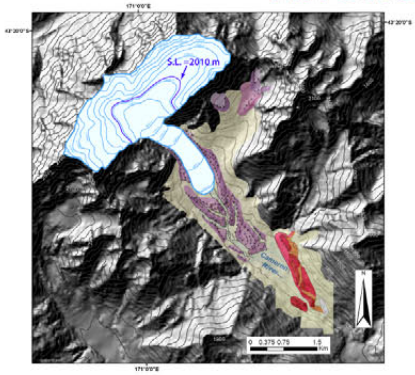

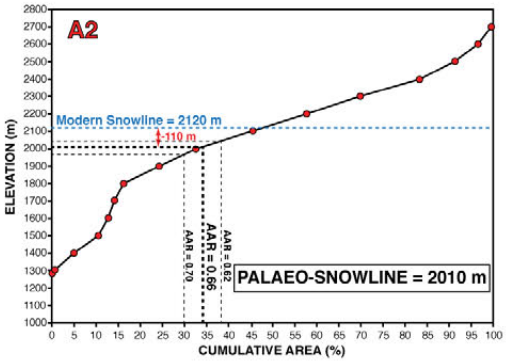

Figure S16 (previous page). Accumulation-area-to-ablation-area ratio (AAR) snowline reconstructions. Left column shows Cameron Glacier surface reconstructions based on catchment and latero-terminal moraine positions and altitudes. Right column shows cumulative area vs. elevation curves. Thick blue lines on glaciers denote reconstructed snowline elevations. Resulting snowlines are given in white boxes.

Using the above methods, we obtained snowline values of 1760 m for the W2 moraine, 1880 m for the C2 moraine, 1980 m for the A4/A3 moraine, and 2010 m for the A2 moraine. These snowlines correspond to depressions below the AD1995 value of 360 m, 240 m, 140 m, and 110 m, respectively. Independent corroboration of these snowline values comes from moraine sets deposited by glaciers located in the adjoining Peg and Lochaber tributary valleys (Fig. S1 and S4). A prominent left-lateral moraine ridge in Lochaber valley, mapped by Burrows[9] as 'Wildman' moraine, can be traced along the south side of the valley to an elevation of 1710 ± 20 m to where it disappears amid ice-smoothed valley-wall topography. This provides a minimum estimate of the snowline of the former south-facing glacier that formed that moraine ridge. The mapping of this moraine ridge as 'Wildman' is supported by the observation that outwash apparently graded to the down-valley end of this moraine ridge extends down-valley to the mouth of Lochaber Stream where it formed a fan, now deeply incised, that was impounded against the Cameron Glacier valley Wildman moraine complex. Thus, the former Cameron Glacier must have stood at the W2 moraine to allow for outwash fan aggradation at the level of the W2 moraine ridge. Deep incision of the Lochaber Stream through the outwash fan and the W2 moraine has occurred since recession of the former Cameron Glaicer from the W2 position. Comparison of snowlines reconstructed using the AAR method for the W2 moraine and using the upper elevation limit of the Lochaber Stream 'W2 correlative' moraine (Figs. S3, S16, S17) yield very similar results.

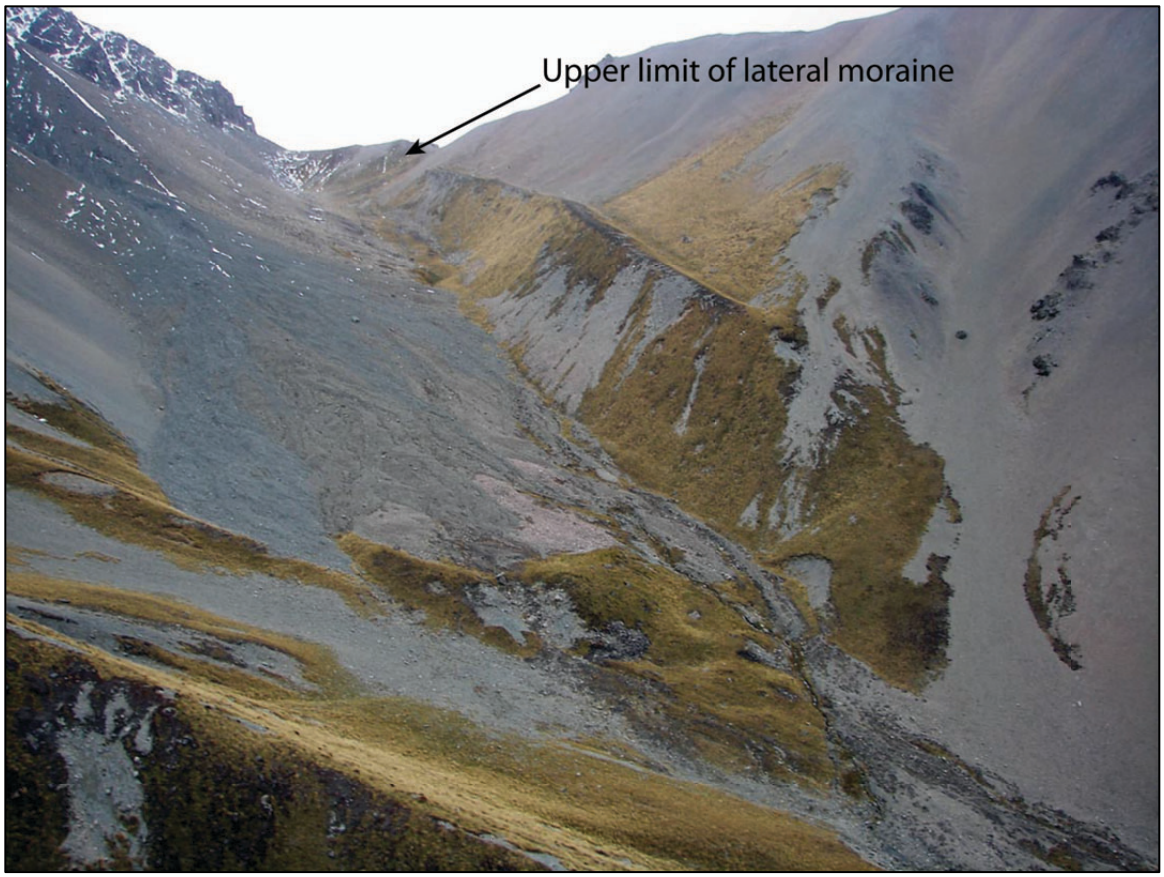

Figure S17. Photograph, vantage northeast, of the Lochaber Stream valley toward the Lochaber left-lateral moraine that has been correlated to the Cameron Glacier Wildman moraines (i.e., 'W') by Burrows[9]. The left-lateral moraine can be traced as high as 1710 m, affording a minimum estimate for the snowline of the glacier that formed the moraine. Imagery date: April, AD2006.

Although the upper limit of the Lochaber lateral moraine affords a minimum estimate for the snowline depression during deposition of the Wildman moraines that is consistent with our estimate derived using the AAR method, the 60-m lower palaeo-snowline measured from the Lochaber left-lateral moraine could also reflect the more southerly aspect of that former glacier compared to the generally more southeastern aspect of the former Cameron Glacier. Indeed, Chinn and Whitehouse[43] reported snowlines of 60 m higher, on average, for SE-facing glacier catchments compared to S-facing glacier catchments. Such an aspect correction would bring the snowline estimates for the former 'Wildman' Cameron and Lochaber valley glaciers into alignment.

A similar independent snowline comparison can be conducted for the A2 reconstruction. A moraine set with very fresh-looking, grey boulders similar in appearance to the A2 moraine exists on the southeast-facing valley wall of the adjoining Peg tributary, just beneath the southeast face of Tent Peak (Fig. S4). The upper limit of the right-lateral moraine of this small glacier system, here referred to as the 'Tent Peak glacier', is 2020 m, and is a minimum altitude for the glacier snowline that formed the moraine. This value is compatible with the upper limit of the Tent Peak glacier 'A2 correlative' moraine agrees well with the 2010 m value (considering the assigned ±50 m systematic uncertainty) obtained from our AAR snowline reconstruction for the Cameron Glacier A2 moraine. Altogether, we observe a close match between AAR-derived snowline reconstructions of W2 and A2 moraines and the upper limits of geomorphologically equivalent lateral moraines of nearby glacier systems. Such independent corroboration reinforces the snowline reconstruction presented here, while also highlighting that an AAR of 0.67 used here is appropriate for generalized reconstruction of former ice tongues via the larger-volume ice model method of Kaplan et al.[20].

Several terminal moraine ridges exist in between those chosen for AAR palaeo-snowline reconstruction, and hence correspond to intermediate palaeo-snowline values. In order to derive snowline information for these moraine ridges, we made use of a strong linear correlation (r^2 = 0.99) between terminal moraine distances along the Cameron valley floor from the A2 moraine ridge and reconstructed palaeo-snowlines given above (Fig. S18). Distances were measured from a fixed reference point at the southernmost extent of the A2 moraine ridge to the southernmost extents of intermediate moraines

along a transect tracking the axis of the valley floor (Fig. S4). The best-fit trend line (Fig. S18) is described by the equation:

Equation S3: y = -72.904x – 110.25

Where the dependent variable, y, is the snowline elevation and the independent variable, x, is the distance along the axis of the valley floor from the A2 moraine ridge. A linear correlation between glacier length and snowline elevation is consistent with observations by Oerlemans[44] for glacier tongues sliding over beds of constant slope. As a test of this relationship, we used the above equation to calculate a snowline value of 2116 m for the AD1989 ice margin mapped by Burrows[9]. This calculated snowline value is in excellent agreement with the reported AD1995 reference equilibrium snowline of 2120 m at Douglas Glacier[4]. Given the tight correlation between snowline and moraine distance, together with accurate reconstruction of the 'modern' (i.e., AD1995 Douglas Glacier) snowline, we consider this conversion of moraine distance to snowline appropriate for reconstructing 'intermediate' moraine snowlines in the Cameron valley.

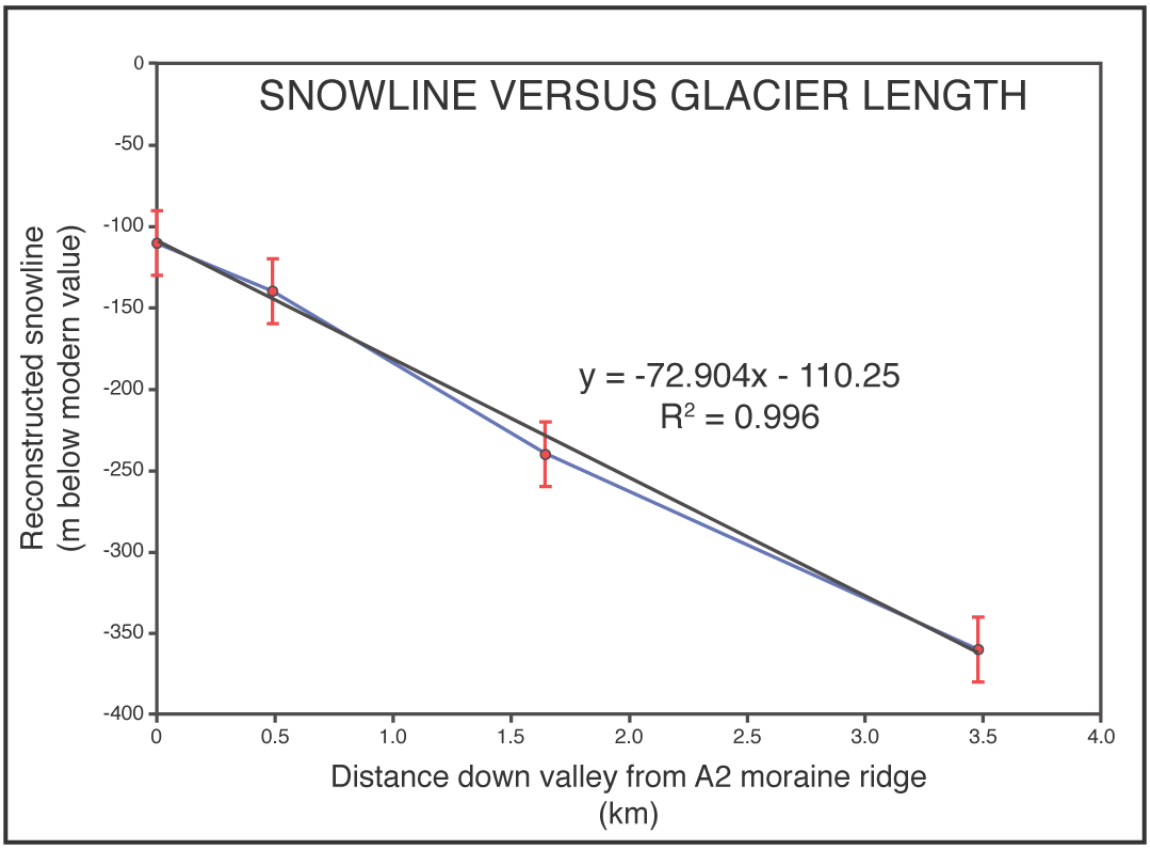

Figure S18. Reconstructed AAR snowlines plotted vs. distance (red dots). Black line is best-fit line. Blue line connects data points. Equation (inset) is used to calculate snowlines for intermediate moraines of the Cameron Glacier system. Nominal ±20 m error bars are shown.

Reconstructed snowline values for all moraine ridges are given in Table S6. Southern Alps glacier snowline elevations are sensitive to variations in atmospheric temperature (e.g., refs.[4,5,45-48]; see also Supplementary section 8.0). Thus, snowlines can be related to temperature via the use of an adiabatic lapse rate. Following Oerlemans[49], we converted snowlines to temperature by using a free-air adiabatic lapse rate of -6.5°C/km. These glacier-inferred temperature departures referenced to the AD1995 value are given in Table S6. As a test of the accuracy of our temperature reconstruction, we compare our reconstructed glacier-inferred temperature anomaly with the National

Institute for Water and Atmospheric Research (NIWA) seven-station instrumental mean-annual temperature series for the period AD1910 to AD2009[50] (Fig. S19). The glacier-inferred temperatures over this time period are based on the observed/dated positions of the Cameron Glacier terminus positions at AD1930, AD1964, AD1989, and AD2006. Figure S19 compares the glacier-inferred temperature reconstruction with the instrumental temperature record. Despite having a low temporal resolution, the reconstructed glacier-inferred temperature rise of 0.83 ± 0.24 °C per century (2σ) since AD1930 agrees well (i.e., within 95% confidence limits) with the strong warming trend shown since the early 20th century in the instrumental data, comprising a recorded mean-annual temperature rise of 0.91 ± 0.3 °C per century. We note that use of alternate adiabatic lapse rates of -5.5°C/km ('moist') and -7.0°C/km ('dry') would result in glacier-inferred warming trends of 0.7 ± 0.20 °C and 0.89 ± 0.29 °C per century, respectively. Within uncertainties, the use of a dry or moist adiabatic lapse rate does not change the overall agreement with the recorded warming trend. However, use of the 'dry' lapse rate of -7.0°C/km to calculate glacier-inferred temperatures gives the best fit to instrumental data.

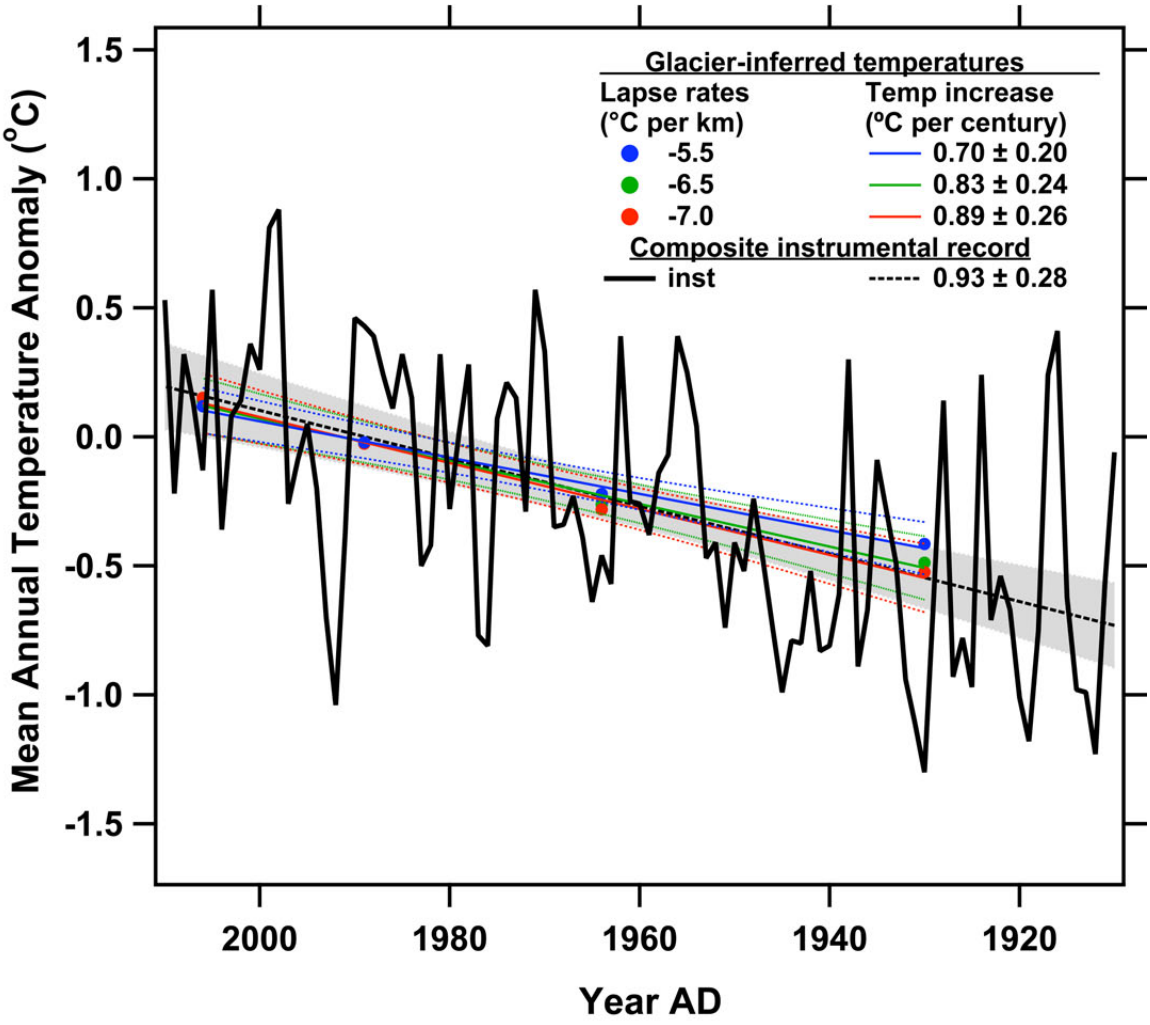

Figure S19. Temperatures reconstructed from glacier snowlines for the instrumental period. Symbols and lines are described in legend (inset). Solid black curve is instrumental temperature anomaly based on the 'Seven Station' series of Mullan et al.[50]. Gray shaded area is the 95% confidence envelope for the instrumental time series. Note the close match between reconstructed and recorded temperature trends over the 20th century.

The implications for instrumental corroboration of our glacier-inferred temperature reconstruction are three-fold. First, these values add further support to the wealth of empirical and theoretical evidence suggesting that atmospheric temperature is the primary control on glacier mass-balance in the Southern Alps, at least on multi-decadal to centurial timescales[45-49,51]. Second, glacier snowline rise has been tracking mean-annual warming since the early AD1900's, highlighting the dominant role of atmospheric temperature on Southern Alps glaciers during the last century. Third, the close correspondence between instrumental temperature data and glacier-inferred temperatures adds confidence to our glacier-inferred reconstruction of atmospheric temperatures for the more distant past.

7.0 Evidence for early Holocene glacier advances elsewhere in the Southern Hemisphere middle latitudes

There is a general paucity of directly age-constrained moraine records of Holocene glacier activity in the Southern Hemisphere middle latitudes. However, Douglass et al.[52] presented evidence for early Holocene glaciation in the southern mid-latitude Andes. When considering the recently updated ^{10}Be production rate for southern South America[30], sixteen ^{10}Be ages on terminal moraine ridges located in the mountains inboard of LGM moraine limits near Fachinal, Chile, place culminations of glacier advance to earliest Holocene time, broadly consistent with the chronology presented for Cameron Glacier. Tentative correspondence between the Cameron Glacier chronology and the chronology of Douglass et al.[52] indicates that cold atmospheric conditions in the

early Holocene may have been a widespread feature of the Southern Hemisphere middle latitudes, consistent with a southward migration of Earth's thermal equator. Further development of precise and accurate chronologies in the Patagonian Andes will be necessary to test the robustness of this correspondence.

8.0 Relationship between Southern Alps glaciers and atmospheric temperature

There is an empirically robust correspondence between snowline elevations and equilibrium line altitudes on Southern Alps glaciers[4,5,43]. Furthermore, glaciological and meteorological analyses have also shown that atmospheric temperature, modulated by circulation patterns, is the dominant climate control on Southern Alps glaciers[4,5,8,42,44-49,51,53-62]. The most recent empirical and theoretical studies to demonstrate the dominance of temperature on glacier mass balance are those of Chinn et al.[42], Purdie et al.[45], and Anderson et al.[46,48]. Moreover, Anderson and Mackintosh[47] showed that temperature change was the dominant driver of Southern Alps glacier behavior during the Holocene and late-glacial time. Given the robust empirical and theoretical links between glacier behavior and atmospheric temperature, established on the basis of over 50 years of detailed glaciological research, we interpret glacier and snowline reconstructions as reflecting past changes in atmospheric temperature.

SUPPLEMENTARY REFERENCES

1 Cox, S. C. & Barrell, D. J. A. Geology of the Aoraki area. *Institute of Geological and Nuclear Sciences 1:250,000 Geological Map 15 GNS Science, Lower Hut, New Zealand*, 1 sheet and 71 pp. (2007).

2 New_Zealand_Meteorological_Service. in *Climatic map series 1:2 000 000* Miscellaneous Publication 175 (New Zealand Meteorological Service, Wellington, 1985).

3 Barrell, D. J. A., Andersen, B. G. & Denton, G. H. *Glacial geomorphology of the central South Island, New Zealand.*, Vol. 27 (GNS Science, 2011).

4 Chinn, T. J. H. Glacier fluctuations in the Southern Alps of New Zealand determined from snowline elevations. *Arctic and Alpine Research* **27**, 187-198 (1995).

5 Clare, G. R., Fitzharris, B. B., Chinn, T. J. H. & Salinger, M. J. Interannual variation in end-of-summer snowlines of the Southern Alps of New Zealand, and relationships with Southern Hemisphere atmospheric circulation and sea surface temperature patterns. *International Journal of Climatology* **22**, 107-120 (2002).

6 Haast, J. V. Watercolour painting (Alexander Turnbull Library, National Library of New Zealand, 1864).

7 Burrows, C. J., Duncan, K. W. & Spence, J. R. Aranuian vegetation history of the Arrowsmith Range, Canterbury II. Revised chronology for moraines of the Cameron Glacier. *New Zealand Journal of Botany* **28**, 455-466 (1990).

8 Chinn, T. J. H. New Zealand glacier response to climate change of the past 2 decades. *Global and Planetary Change* **22**, 155-168 (1999).

9 Burrows, C. J. Late Pleistocene and Holocene moraines of the Cameron Valley, Arrowsmith Range, Canterbury, New Zealand. *Arctic and Alpine Research* **7**, 125-140 (1975).

10 Burrows, C. J. *Julius Haast in the Southern Alps*. (Canterbury University Press, 2005).

11 Barrell, D. J. A. in *Quaternary Glaciations - Extent and chronology, Part IV - a closer look* Vol. 15 *Developments in Quaternary Science* (eds J. Ehlers, P.L. Gibbard, & P.D. Hughes) Ch. 75, 1047-1064 (Elsevier, 2011).

12 Mabin, M. C. G. Late Pleistocene glacial sequence in the Lake Heron basin, mid-Canterbury. *New Zealand Journal of Geology and Geophysics* **27**, 191-202 (1984).

13 Birkeland, P. W. Subdivision of Holocene glacial deposits, Ben Ohau Range, New Zealand, using relative-dating methods. *Geological Society of America Bulletin* **93**, 443-449 (1982).

14 Putnam, A. E. *et al.* Glacier advance in southern middle latitudes during the Antarctic Cold Reversal. *Nature Geoscience* **3**, 700-704 (2010).

15 Bronk Ramsay, C. Development of the radiocarbon calibration program Oxcal. *Radiocarbon* **43**, 255-363 (2011).

16 Reimer, P. J. *et al.* INTCAL09 and MARINE09 radiocarbon age calibration curves, 0-50,000 years cal BP. *Radiocarbon* **51**, 1111-1150 (2009).

17 McCormac, F. G. *et al.* SHCal04 Southern Hemisphere calibration, 0 - 11.0 cal kyr BP. *Radiocarbon* **46**, 1087-1092 (2004).

18 Schaefer, J. M. *et al.* High-frequency Holocene glacier fluctuations in New Zealand differ from the northern signature. *Science* **324**, 622-625 (2009).
19 Putnam, A. E. *et al.* In situ cosmogenic ^{10}Be production-rate calibration from the Southern Alps, New Zealand. *Quaternary Geochronology* **5**, 392-409 (2010).
20 Kaplan, M. R. *et al.* Glacier retreat in New Zealand during the Younger Dryas stadial. *Nature* **467**, 194-197 (2010).
21 Winkler, S. & Matthews, J. A. Holocene glacier chronologies: Are 'high-resolution' global and inter-hemispheric comparisons possible? *The Holocene* **20**, 1137-1147 (2010).
22 Kelly, M. A. *The Late Würmian Age in the western Swiss Alps - Last glacial maximum (LGM) ice-surface reconstruction and ^{10}Be dating of late-glacial features* Ph.D. dissertation thesis, University of Bern, (2003).
23 Nishiizumi, K. *et al.* Absolute calibration of ^{10}Be AMS standards. *Nuclear Instruments and Methods in Physics Research B* **258**, 403-413 (2007).
24 Lal, D. Cosmic-ray labeling of erosion surfaces: in situ nuclide production rates and erosion models. *Earth and Planetary Science Letters* **104**, 424-439 (1991).
25 Stone, J. O. Air pressure and cosmogenic isotope production. *Journal of Geophysical Research* **105**, 23753-23759 (2000).
26 Lifton, N. *et al.* Addressing solar modulation and long-term uncertainties in scaling secondary cosmic rays for in situ cosmogenic nuclide applications. *Earth and Planetary Science Letters* **239**, 140-161 (2005).
27 Lifton, N., Smart, B. & Shea, M. Scaling time-integrated in situ cosmogenic nuclide production rates using a continuous geomagnetic model. *Earth and Planetary Science Letters* **268**, 190-201 (2008).
28 Dunai, T. Influence of secular variation of the magnetic field on production rates of in situ produced cosmogenic nuclides. *Earth and Planetary Science Letters* **193**, 197-212 (2001).
29 Desilets, D., Zreda, M. & Prabu, T. Extended scaling factors for in situ cosmogenic nuclides: new measurements at low latitude. *Earth and Planetary Science Letters* **246**, 256-276 (2006).
30 Kaplan, M. R. *et al.* In-situ cosmogenic ^{10}Be production rate at Lago Argentino, Patagonia: Implications for late-glacial climate chronology. *Earth and Planetary Science Letters* **309**, 21-32 (2011).
31 Fenton, C. R. *et al.* Regional 10Be production rate calibration for the past 12 ka deduced from two radiocarbon-dated rock avalanches at 69°N, Norway. *Geophysical Research Abstracts* **12**, EGU2010-11702-11702 (2010).
32 Briner, J. P., Young, N. E., Goehring, B. M. & Schaefer, J. M. Constraining Holocene 10Be production rates in Greenland. *Journal of Quaternary Science* **27**, 2-6 (2011).
33 Balco, G. & Schaefer, J. M. Cosmogenic-nuclide and varve chronologies for the deglaciation of southern New England. *Quaternary Geochronology* **1**, 15-28 (2006).
34 Bevington, P. & Robinson, D. *Data Reduction and Error Analysis for the Physical Sciences*. (WCB McGraw Hill, 1992).
35 Dunai, T. J. *Cosmogenic Nuclides: Principals, Concepts, and Applications in the Earth Surface Sciences*. (Cambridge University Press, 2010).

36 Grubbs, F. E. Procedures for detecting outlying observations in samples. *Technometrics* **11**, 1-21 (1969).
37 Lowell, T. V. *et al.* Rhizocarpon calibration curve for the Aoraki/Mount Cook area of New Zealand. *Journal of Quaternary Science* **20**, 313-325 (2005).
38 Denton, G. H. & Broecker, W. S. Wobbly ocean conveyor circulation during the Holocene? *Quaternary Science Reviews* **27**, 1939-1950, doi:10.1016/j.quascirev.2008.08.008 (2008).
39 Burrows, C. J., Bell, D. & Grant, H. Two new radiocarbon ages for mid- and late-Aranui age valley-train deposits of the Franz Josef Glacier, Westland, New Zealand. *Journal of the Royal Society of New Zealand* **32**, 415-425 (2002).
40 Klok, E. J. & Oerlemans, J. Climate reconstructions derived from global glacier length records. *Arctic, Antarctic, and Alpine Research* **36**, 575-583 (2004).
41 Porter, S. C. Snowline depression in the tropics during the Last Glaciation. *Quaternary Science Reviews* **20**, 1067-1091 (2001).
42 Chinn, T. J. H. Annual Ice Volume Changes 1976-2008 for the New Zealand Southern Alps. *Global and Planetary Change*, doi:10.1016/j.gloplacha.2012.04.002 (2012).
43 Chinn, T. J. H. & Whitehouse, I. E. in *World Glacier Inventory* Vol. 126 219-228 (International Association of Hydrological Sciences Publication, 1980).
44 Oerlemans, J. *Minimal Glacier Models*. 2nd edn, (igitur, Utrecht Publishing & Archiving Services, 2011).
45 Purdie, H. *et al.* Interannual variability in net accumulation on Tasman Glacier and its relationship with climate. *Global and Planetary Change* doi: 10.1016/j.gloplacha.2011.04.004 (2011).
46 Anderson, B., Lawson, W., Owens, I. & Goodsell, B. Past and future mass balance of 'Ka Roimata o Hine Hukatere' Franz Josef Glacier, New Zealand. *Journal of Glaciology* **52**, 597-607 (2006).
47 Anderson, B. & Mackintosh, A. Temperature change is the major driver of late-glacial and Holocene glacier fluctuations in New Zealand. *Geology* **34**, 121-124 (2006).
48 Anderson, B. *et al.* Climate sensitivity of a high-precipitation glacier in New Zealand. *Journal of Glaciology* **56**, 114-128 (2010).
49 Oerlemans, J. Climate sensitivity of Franz Josef Glacier, New Zealand, as revealed by numerical modelling. *Arctic and Alpine Research* **29**, 233-239 (1997).
50 Mullan, A. B., Stuart, S. J., Hadfield, M. G. & Smith, M. J. Report on the review of NIWA's 'Seven-Station' Temperature Series. *NIWA Information Series* **78**, 175 p. (2010).
51 Anderson, B. Interactive comment on "Synoptic climate change as a driver of late Quaternary glaciations in the mid-latitudes of the Southern Hemisphere" by H. Rother and J. Shulmeister. *Climate of the Past Discussions* **1**, S161-S167 (2005).
52 Douglass, D. C. *et al.* Evidence of early Holocene glacial advances in southern South America from cosmogenic surface-exposure dating. *Geology* **33**, 237-240 (2005).
53 Chinn, T. J. New Zealand glacier responses to climate change of the past century. *New Zealand Journal of Geology and Geophysics* **39**, 415-428 (1996).

54 Fitzharris, B. B., Clare, G. R. & Renwick, J. Teleconnections between Andean and New Zealand glaciers. *Global and Planetary Change* **59**, 159-174 (2007).
55 Hooker, B. L. & Fitzharris, B. B. The correlation between climatic parameters and the retreat and advance of Franz Josef Glacier, New Zealand. *Global and Planetary Change* **22**, 39-48 (1999).
56 Tyson, P. D., Sturman, A. P., Fitzharris, B. B., Mason, S. J. & Owens, I. F. Circulation changes and teleconnections between glacial advances on the west coast of New Zealand and extended spells of drought years in South Africa. *International Journal of Climatology* **17**, 1499-1512 (1997).
57 Fitzharris, B. B., Chinn, T. J. & Lamont, G. N. Glacier balance fluctuations and atmospheric circulation patterns over the Southern Alps, New Zealand. *International Journal of Climatology* **17**, 745-763 (1997).
58 Harrington, H. J. Glacier wasting and retreat in the Southern Alps of New Zealand. *Journal of Glaciology* **2**, 140-144 (1952).
59 Oerlemans, J. Extracting a Climate Signal from 169 Glacier Records. *Science* **308**, 675-677 (2005).
60 Hoelzle, M. *et al.* The application of glacier inventory data for estimating past climate change effects on mountain glaciers: A comparison between the European Alps and the Southern Alps of New Zealand. *Global and Planetary Change* **56**, 69-82 (2007).
61 Salinger, M. J. On the suggestion of post-1950 warming over New Zealand. *New Zealand Journal of Science* **25**, 77-86 (1982).
62 Salinger, M. J. & Mullan, A. B. New Zealand climate: Temperature and precipitation variations and their links with atmospheric circulation 1930-1994. *International Journal of Climatology* **19**, 1049-1071 (1999).